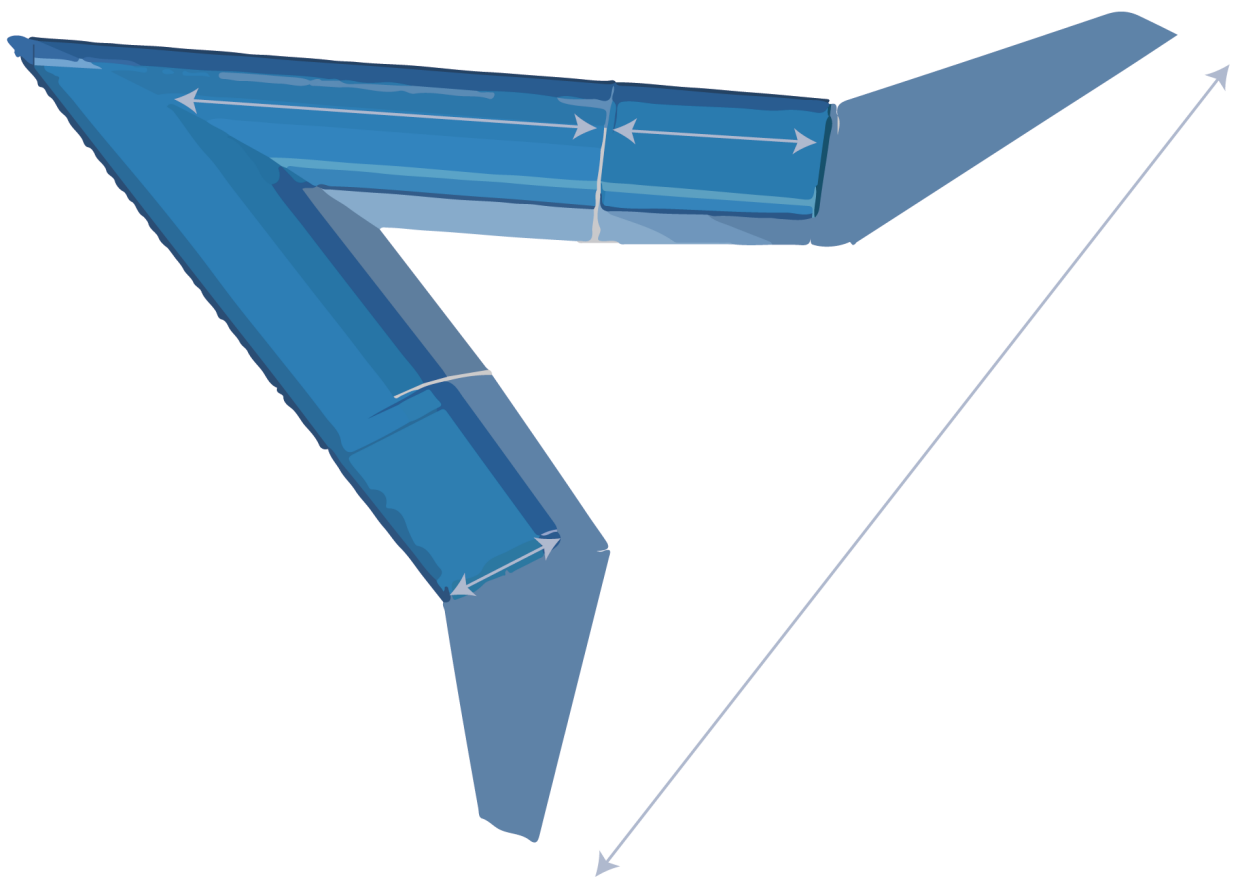


# Parametrisation of the Flying-V Outer Mould Line

M. Hillen

Technische Universiteit Delft





# Parametrisation of the Flying-V Outer Mould Line

by

**M. Hillen**

in partial fulfillment of the requirements for the degree of

**Master of Science**  
in Aerospace Engineering

at the Delft University of Technology,  
to be defended publicly on Wednesday September 30, 2020 at 1:00 PM.

Equivalent number of words:	20,488	
Thesis committee:	Dr. ir. R. Vos,	TU Delft, supervisor
	Dr. ir. L.L.M. Veldhuis,	TU Delft
	Dr. ing. S.G.P. Castro,	TU Delft
	Ir. P. Proesmans,	TU Delft

An electronic version of this thesis is available at <http://repository.tudelft.nl/>.



# Summary

The Flying-V, a flying wing aircraft concept, is being designed to carry passengers and cargo. The wing design is built around two cylindrical semi pressure cabins positioned with a high sweep angle to create a V shape. The objective of the research presented in this thesis is to create a parametrisation of the Flying-V outer mould line that includes cabin design flexibility and manufacturability, and that can be used in an aerodynamic optimisation routine. To include cabin design flexibility, a fuselage parametrisation is created that exists of several oval cross-section fuselage trunks for which the length, width, and several height parameters can be specified. The outer mould line shape strongly depends on the fuselage shape, because in the geometry generation process the latter is an input for the former. Manufacturability is included by introducing a constant cross-section wing- and fuselage trunk and by mainly using linear lofted wing trunks. The parametrisation is coupled with an aerodynamic analysis tool to facilitate future aerodynamic optimisations.

The robustness of the parametrisation is evaluated by sampling the design space and evaluating per sample whether the shape violates the proposed constraints. This sampling study resulted in a robustness, expressed as the feasible domain coverage of the design space, of 29 %. To increase the robustness, a different rear aerofoil parametrisation is recommended.

In addition to the quantitative robustness study, a qualitative demonstration of the parametrisation is done in the form several case studies. The first case study is a Flying V that is generated with the proposed parametrisation, but with the same cabin- and planform characteristics of the former Flying-V design. This case study reveals that the major difference between the proposed and the former parametrisation is the orientation of the smoothness discontinuities, and that this causes higher adverse pressure gradients over the wing surface. The lift-to-drag ratio of this configuration is 13% lower than that of the former Flying-V design. The drag is calculated using the Euler equations of the Stanford University Unstructured software supplemented with a viscous drag estimation based on semi-empirical relations.

The other case studies have larger fuselages compared to the first case, while maintaining the same aerofoil thickness in the outboard wing. This causes a region of the outer mould line that has abrupt curvature changes in the butt plane curves. The lift-to-drag ratio of a Flying-V with the same span as the former design but with a larger cabin, is 32% lower than the former design. This indicates that the increased cabin size also has a high impact on the aerodynamic efficiency of the aircraft. However, to actually draw a reasonably valid comparison between a shape that is generated with the proposed parametrisation, first an optimisation needs to be carried out.



# Preface

This thesis is the final part that I am required to hand in in order to complete my Master's degree. There are a couple of people that I would like to thank, because they have helped me during this final part of the Master programme. First of all, I would like to thank Roelof Vos, who was my supervisor during this project. He invested time in helping me and he gave me helpful feedback during our bi-weekly meetings. I am also grateful that he invited me to join a radio broadcast about the Flying-V, and the innovation fair at KLM! Those were both nice experiences. Next, I would also like to thank my Aerospace Engineering friends, with whom I could always talk about study related topics and, more importantly, have a nice time while studying in Delft. Of these friends, Colin Heimans and Robin Piet deserve special thanks; Colin helped me many times with my programming questions and Robin because he was a nice study partner from the start of the bridging programme until the end of the master. Lastly, I would like to thank my parents, Ans Witte and Johan Hillen, who have been there for me throughout my whole study, and my boyfriend, Lars Koel, who is always understanding and supportive!

*M. Hillen*  
*Delft, September 2020*



# Contents

<b>Summary</b>	<b>iii</b>
<b>List of Figures</b>	<b>ix</b>
<b>List of Tables</b>	<b>xi</b>
<b>Nomenclature</b>	<b>xiii</b>
<b>1 Introduction</b>	<b>1</b>
1.1 Problem indication / Purpose	1
1.2 Problem statement	3
1.3 The scope of the study	3
1.4 Research method	3
1.5 Relevance	4
1.6 Thesis outline	4
<b>2 Design for manufacturing</b>	<b>5</b>
2.1 Manufacturability	5
2.2 Double curvature	5
2.3 Part variety and part count	6
<b>3 Geometry parametrisation method</b>	<b>7</b>
3.1 Lofted surfaces	8
3.2 Fuselage	8
3.2.1 Fuselage cross-section	8
3.2.2 Fuselage planform	10
3.3 Wing	11
3.3.1 Inboard aerofoil: an oval fuselage cross-section extended with a rear aerofoil	11
3.3.2 Wing outboard aerofoils	13
3.3.3 Wing planform	13
3.3.4 Twist and dihedral	16
3.4 Geometry evaluation	16
<b>4 Aerodynamic analysis method</b>	<b>19</b>
4.1 Euler analysis	19
4.1.1 Mesh	20
4.1.2 Configuration	21
4.1.3 Verification	22
4.2 Viscous drag estimation	23
4.2.1 Form factor	23
4.2.2 Viscous drag	23
4.2.3 Limitations of this method	24
<b>5 Results</b>	<b>25</b>
5.1 Robustness of the geometry parametrisation	25
5.1.1 Design space	25
5.1.2 Sampling	25
5.2 Case studies	27
5.2.1 Case 1 - an approximation of Faggiano's design	28
5.2.2 Case 2 - a Flying-V-800	29
5.2.3 Case 3 - a Flying-V-900	30
5.2.4 Case 4 - a Flying-V-1000	31

---

<b>6</b>	<b>Conclusions and recommendations</b>	<b>35</b>
6.1	Conclusions . . . . .	35
6.2	Recommendations . . . . .	36
	<b>Bibliography</b>	<b>37</b>
<b>A</b>	<b>Class diagram</b>	<b>39</b>
<b>B</b>	<b>Input files</b>	<b>41</b>
<b>C</b>	<b>Mesh convergence</b>	<b>47</b>
<b>D</b>	<b>Design variables and their bounds</b>	<b>49</b>
<b>E</b>	<b>Design space impression</b>	<b>51</b>

# List of Figures

1.1	Streamwise oval and wing shapes of the Flying-V design of Faggiano and Van der Schaft	2
1.2	Primary structure concept of Van der Schaft. Reprinted from <i>Development, Model Generation and Analysis of a Flying V Structure Concept</i> [1]	2
2.1	Core Manufacturability Concepts [2]	6
3.1	Unified Modeling Language (UML) class diagram of the main Flying-V components	7
3.2	UML class diagram of the different trunks	8
3.3	Oval fuselage cross-section parametrisation	9
3.4	three-dimensional visualisation of a semi fuselage	10
3.5	Fuselage planform parameters	11
3.6	UML class diagram of the wing component	12
3.7	Inboard aerofoil drawing in its own $xz$ plane	12
3.8	(semi-) Wing planform parametrisation	14
3.9	Wing planform angles	15
4.1	UML class diagram of the aerodynamic analysis module	20
4.2	Inviscid drag coefficient for different mesh refinements, $M = 0.85$ , $C_L = 0.266$	20
4.3	An example of a coarse surface grid (not the default grid)	21
4.4	Boundaries of the computational domain	22
4.5	Pressure coefficient contour plots over the top surface of the current Flying-V geometry	22
5.1	Convergence of Latin Hypercube Sampling (LHS) sample size	26
5.2	Wing planform shapes of the (not yet optimised) Flying-V family	27
5.3	Comparison of Flying-V planform shapes between the Faggiano parametrisation and the proposed parametrisation	29
5.4	Semi wing geometry of case 1, with a streamwise cut at $0.6\frac{b}{2}$	29
5.5	Case 1 $C_p$ , $Ma = 0.85$ , $C_L = 0.266$	30
5.6	Former Flying-V OML $C_p$ contours, $Ma = 0.85$ , $C_L = 0.266$	30
5.7	Flying-V-800 planform, courtesy of R. Vos	30
5.8	Semi wing geometry of case 2, with a streamwise cut at $0.4\frac{b}{2}$	31
5.9	Flying-V-800 $C_p$ contours, $Ma = 0.85$ , $C_L = 0.27$	31
5.10	Flying-V-900 planform, courtesy of R. Vos	32
5.11	Flying-V-900 $C_p$ contours, $Ma = 0.85$ , $C_L = 0.266$	33
5.12	Flying-V-900 Mach contours, $Ma = 0.85$ , $C_L = 0.266$	33
5.13	Flying-V-1000 planform, courtesy of R. Vos	33
5.14	Flying-V-1000 with two different section 4 shapes	34
5.15	Flying-V-1000 $C_p$ contours, $Ma = 0.85$ , $C_L = 0.266$	34



# List of Tables

3.1	Oval fuselage section input parameters . . . . .	9
3.2	Fuselage planform input parameters . . . . .	11
3.3	Inboard aerofoil parameters . . . . .	13
3.4	Outboard aerofoil parameters . . . . .	14
3.5	Wing planform parameters . . . . .	15
3.6	Outboard aerofoil parameters . . . . .	16
4.1	Default grid controlling parameters . . . . .	21
4.2	Coefficients of two SU2 version results with the current Flying-V design's geometry . . . . .	22
5.1	Fixed input parameters for sampling study . . . . .	26
5.2	Geometrical properties of the current Flying-V design . . . . .	27
5.3	Aerodynamic coefficients of the different cases . . . . .	28
B.1	Input parameters of case 1: an approximation of Faggiano's geometry . . . . .	42
B.2	Input parameters of case 2: a Flying-V-800 . . . . .	43
B.3	Input parameters of case 2: a Flying-V-900 . . . . .	44
B.4	Input parameters of case 2: a Flying-V-1000 . . . . .	45
C.1	Mesh convergence inputs . . . . .	47



# Nomenclature

## Roman

$\bar{c}$	Normalised chord
$\bar{x}_s$	Normalised starting location of a rear aerofoil curve
$\mathbb{R}$	The set of real numbers
$\mathbb{X}$	Design space
$\mathbf{g}$	Inequality constraint vector
$\mathbf{h}$	Equality constraint vector
$\mathbf{x}$	Design vector
$ff$	Form factor
$Ma$	Mach number
$Re$	Reynolds number
$A$	Area
$A$	List of Bernstein coefficients
$a$	Polynomial coefficient
$b$	Wing span
$c$	Chord, or polynomial coefficient for the fourth order term
$c'$	Planform chord length
$C_D$	Three dimensional drag coefficient
$c_d$	Drag coefficient of a wing section
$C_F$	Flat plate skin friction coefficient
$C_p$	Pressure coefficient
$H_1$	Oval crown height
$H_2$	Oval cabin height
$H_3$	Oval keel height
$H_w$	Oval height of input width
$i$	Section incidence angle
$k$	Skin roughness value
$L$	Centre line length (with respect to the fuselage)
$l$	Planform leading edge length, or characteristic length
$N$	Number of samples

$n$	Number of design variables
$S$	Wing area
$w_{\text{oval}}$	Oval width
$w_H$	Oval width at input height
$x$	Aircraft longitudinal axis, unless otherwise indicated
$x_s$	Starting location of a rear aerofoil curve, measured from inboard aerofoil origin
$y$	Aircraft lateral axis, unless otherwise indicated
$z$	Aircraft top axis, unless otherwise indicated
mac	Mean Aerodynamic Chord

### Greek

$\delta$	Orientation angle of section 4
$\epsilon$	Error
$\Gamma$	Dihedral of leading edge
$\Lambda$	Leading edge sweep angle
$\lambda$	Taper ratio
$\Lambda_{\frac{1}{2}}$	Half chord sweep angle
$\Lambda_i$	$i = 1, 2, 3$ : Trailing edge sweep
$\mu$	Angle of revolution for the toroidal connection trunk

### Subscripts

2	Section 2, or trunk 2
4	Section 4, or trunk 4 (for a dihedral or length parameter)
$r$	Root
$t$	Tip
1	Section 1, or untapered trunk (for a length parameter), or oval crown height(for a $H$ )
3	Section 3, or most inboard tapered trunk (for a length parameter), or oval crown height(for a $H$ )
3	Section 3, or trunk 3
in	Inboard wing
inv	Inviscid
low	Lower rear aerofoil curve
out	Outboard wing
TE	Trailing edge
up	Upper rear aerofoil curve
visc	Viscous

# 1

## Introduction

In aircraft design, one of the main objectives is to achieve a low fuel consumption. One factor that contributes to obtaining a low fuel consumption is a high aerodynamic efficiency, or low aerodynamic drag. A flying wing is an aircraft configuration that does not carry the payload in a separate fuselage, but carries it inside the wing. Therefore there is no need for a separate fuselage that, from an aerodynamic point of view, only increases drag. Omitting the fuselage decreases the wetted area to volume ratio and therefore increases the lift-to-drag ratio by an estimated 20% compared to a conventional aircraft. [3].

The Flying-V is a promising flying wing configuration that has a potentially large increase in fuel efficiency compared to a similar capacity conventional aircraft. It has a V shape that results from arranging two semi-wings at a high sweep angle, and placing the fuselage inside the front of the wing, along the leading edge. The Flying-V was conceptualised by Benad (2015) [4] to have an as high as possible lift-to-drag ratio and low mass. His design was estimated to have a 10 % higher lift-to-drag ratio and 2 % lower mass than its reference conventional aircraft, the A350-900.

Delft University of Technology continues to research the Flying-V in the form of aerodynamic and structural design and analysis [1, 5, 6], engine integration studies [7], and wind tunnel tests [8, 9]. Faggiano (2016) [5] carried out an aerodynamic optimisation, which resulted in an improved aerodynamic design compared to that of Benad. The main differences between Faggiano's and Benad's design are an increased sweep angle of the outboard wing, and a fuselage design that is based on the oval cross-section of Hoogreef (2012) [10] instead of a circular cross-section. Faggiano's Flying-V is estimated to be 25 % more aerodynamically efficient than the NASA Common Research Model.

### 1.1. Problem indication / Purpose

The geometrical model that Faggiano used for the aerodynamic design can be improved. Some of the issues that can be improved are outlined in this section.

First of all, the area and volume of the fuselage's passenger and cargo compartments were based on typical values outlined by Raymer (2012) [11]. Modelling of the positions of the passenger seats, galleys, lavatories, doors, and cargo containers revealed that the total cabin area is too small to position all the payload in the fuselage.

Secondly, Faggiano's parametrisation has excess space between the tapered fuselage trunk and the Outer Mould Line (OML). This can be unnecessarily complicated to manufacture, because it requires two skins (one for the fuselage, and one for the wing) in close proximity to each other, while one skin is sufficient.

Thirdly, near the root of the wing, the fuselage does not fit inside the OML. This is illustrated in [Figure 1.1](#), which shows a streamwise cut through the fuselage and wing, near the root. Since the wing OML shape is submitted to the aerodynamic analysis, a modelling error introduced; the protrusion of the fuselage is not taken into account.

Fourthly, the OML does not reflect the proposed primary structural design any more. The structural design of Van der Schaft ([Figure 1.2](#)) positioned the ribs of the rear wing as extensions of the cabin frames, which is perpendicular to the leading edge [1]. The wing OML is a compound of several wing

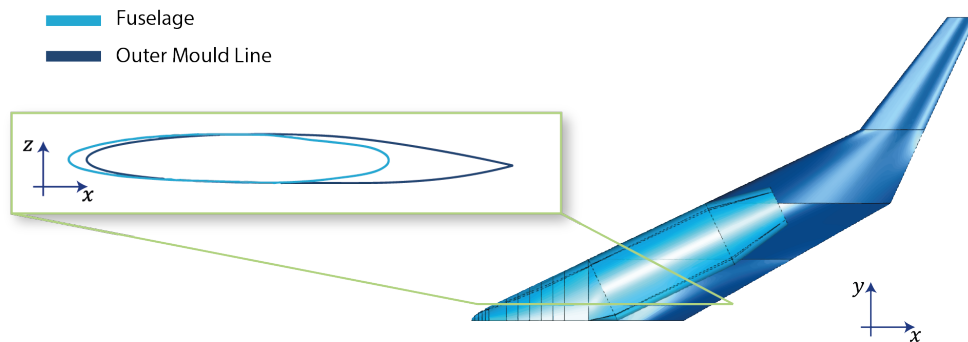


Figure 1.1: Streamwise oval and wing shapes of the Flying-V design of Faggiano and Van der Schaft

trunks. These wing trunks are linear lofts between streamwise profiles. This method of constructing the OML results in smoothness discontinuities at these streamwise profiles. To recreate this shape, structural members have to be placed along these streamwise kinks, which contradicts the structural design by Van der Schaft.

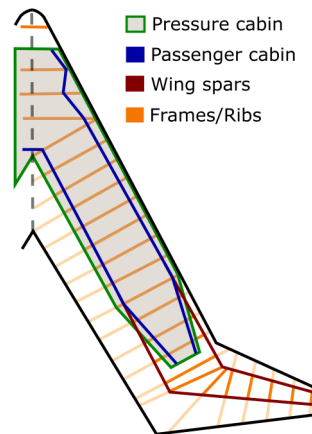


Figure 1.2: Primary structure concept of Van der Schaft. Reprinted from *Development, Model Generation and Analysis of a Flying V Structure Concept* [1]

Fifth, the wing trunks of the current design are all tapered. Although wing taper has aerodynamic and structural benefits, from a manufacturability point of view an untapered wing is preferred over a tapered wing. The explanation for this is that the tapered wing has a varying cross-section, meaning that every rib would have different dimensions. One of the basic principles of design for manufacturing, is to reduce number and the variety of parts in an assembly [12, 13]. In addition, a constant cross-section creates the possibility to stretch or shrink the fuselage and wing, which facilitates the design of a family of Flying-V's.

Sixth, it turned out that structural reinforcements are required at the root. Simultaneous to the aerodynamic design of the OML, the structural design was addressed by Van der Schaft (2017) [1] and subsequently by Claeys (2018) [6]. Van der Schaft positioned the fuselage frames near the root perpendicular to the direction of flight. Claeys found that this is insufficient to carry the torsional loads and proposed structural reinforcements. The benefit of having the structural frames oriented orthogonal to the longitudinal axis, and not in the symmetry plane, was to have more openness of the cabin. Since this turned out to be unrealistic, and a structure in the symmetry plane is nonetheless required, the fuselage design near the root does not require the oval frames to be positioned orthogonal to the aircraft longitudinal axis any more.

Based on these findings, the following parametrisation requirements are proposed with the aim to include cabin design flexibility and manufacturability into the aerodynamic design:

1. Include cabin design flexibility to allow resizing of the cabin

2. Omit of skin-in-skin design
3. Make sure the fuselage fits inside the wing
4. Position the loft profiles in the same planes as the structural frames
5. Include an untapered fuselage- and wing trunk
6. Omit the orthogonal to free-stream orientation of the profiles near the root

## 1.2. Problem statement

It is evident that addressing the issues discussed in the previous section will result in a different parametrisation of the OML. Naturally, one would be interested in the aerodynamic performance of the renewed OML, and thus the parametrisation should also be admissible to aerodynamic analyses. Hence the research objective of this study is *to create a new parametrisation of the Flying-V Outer Mould Line that includes cabin design flexibility and manufacturability, and that can be used in an aerodynamic design optimisation routine*. To achieve this objective, the main research question will be answered, which is:

What is the Flying-V OML parametrisation that results from the manufacturability and design flexibility requirements stated in the previous section?

The following three research questions support the main research question.

1. What are the differences between the proposed parametrisation and the former parametrisation?
2. How suitable is the proposed parametrisation for an aerodynamic analysis?
3. How robust is the proposed parametrisation?

## 1.3. The scope of the study

The research object is the Flying-V. Therefore, the parametrisation that is built is a model for the Flying-V and not for a generic flying wing. Also, while this research aims to provide a basis that can be used in an aerodynamic optimisation, the optimisation itself is not carried out.

Furthermore, the shape that is required for aerodynamic analysis is the OML. While on an abstract level (by deciding the orientation of the wing loft profiles) the structural design is taken into account, the aircraft structure is not actually modelled. The fuselage defines the OML shape and therefore the fuselage shell is included in the parametrisation as well. In this thesis, the term OML refers to that of the *wing*. Engines, winglets, and movables are not included.

All aerodynamic analyses carried out are based on cruise conditions, because of the aim to use the parametrisation in an aerodynamic optimisation to optimise the aerodynamic efficiency. Cruise is the most relevant stage of flight to optimise for aerodynamic efficiency, because it is the largest part of the aircraft's mission. For the Flying-V this means an altitude of 13,000 meters, a cruise Mach number of 0.85, and a lift coefficient of 0.266 [5]. The flow conditions, such as speed of sound and density, are based on the International Standard Atmosphere (ISA).

## 1.4. Research method

To answer the first research question, a new parametrisation is created, which is also stated in the research objective. To create the parametrisation, an engineering application is created using Python in combination with the ParaPy toolkit. The ParaPy toolkit contains libraries that allow 3-dimensional geometry modelling. The first research question also aims to compare the new proposed parametrisation to that of Faggiano. To draw this comparison, a Flying-V shape is created, using the proposed parametrisation, that approximates Faggiano's design in terms of planform shape, fuselage shape, and wing area.

To create a parametrisation that includes cabin design flexibility and manufacturability, the requirements stated in [section 1.1](#) are included.

Next to these rules for the geometry parametrisation, the application should be admissible to an aerodynamic optimisation routine. This requires that the application can compute the objective function, which is often the lift-to-drag ratio in cruise conditions [14]. To compute the lift-to-drag ratio, communication rules with an aerodynamic solver are established. Faggiano's aerodynamic design has been created using an aerodynamic optimisation that employed the Euler analysis of Stanford University Unstructured (SU2) in combination with semi-empirical relations to compute the lift-to-drag ratio [5]. A lot of SU2 communication rules, as well as the semi-empirical relations, are re-used in the proposed application. To determine how suitable the proposed parametrisation is for an aerodynamic analysis, the aerodynamic results of a number of cases are evaluated.

The third research question aims to show how robust the parametrisation is. This is determined by sampling the design space and evaluating per sample whether it results in a feasible shape. A low robustness means that a large portion of the design space is covered by infeasible designs.

## 1.5. Relevance

This research serves as a preparation for an aerodynamic optimisation. An engineering application is an excellent tool to use for optimisation because it automates the design tasks (geometry generation and aerodynamic analysis in this case). If such an optimisation is carried out, its result would be a new Flying-V design that complies with the aforementioned requirements of cabin design flexibility and manufacturability. This new design, when compared to the that of Faggiano (2016), could provide insight in the effect of this change in parametrisation on the aerodynamic performance of the Flying-V. Based on that, further design decisions can be made.

## 1.6. Thesis outline

chapter 2 provides some theoretical background information about Design For Manufacturing (DFM). The parametrisation of the Flying-V OML is still on quite an abstract level, because it is still in the early design stage of the aircraft. Still, the basic principles of DFM are included in the parametrisation. The parametrisation is implemented in a design application. That application has a geometry module and an aerodynamic analysis module. The geometry parametrisation itself is explained in chapter 3. The aerodynamic analysis module that is included in the design application is described in chapter 4. In chapter 5, the results are presented in the form of an assessment of the robustness of the geometry parametrisation, and a the evaluation of the geometries and aerodynamic results of a number of case studies. In the final chapter, chapter 6, the research questions are answered and recommendations for future work are presented.

# 2

## Design for manufacturing

With an estimated lift-to-drag ratio of 23.7, which is 25% higher than that of the NASA common research model [5], the Flying-V concept is promising. Ideally this comparison is done with the A350-900, because it is a state-of-the-art tube-and-wing aircraft with the same capacity and cruise-speed as the Flying-V [4]. Because the A350 data were unavailable for Faggiano, he compared the Flying-V to the NASA common research model. However, a preliminary (or conceptual) aircraft design is not equally comparable to an existing aircraft, because there are matters which are not addressed during the preliminary analysis [15]. One of the aspects in which the preliminary design can turn out to have poor performance is manufacturability. The existing aircraft design (e.g. the A350) has already been manufactured and manufacturing issues have been resolved or accepted, which have likely resulted into increased weight, or cost, or aerodynamic performance reduction [16]. The conceptual or preliminary design (e.g. the Flying-V) is only an abstract concept and if manufacturability is not taken into account at all, it makes the comparison less valid. Therefore, a logical next step in the design process of the Flying-V, is to address manufacturability. DFM is a methodology that not only focuses on the functionality of the product, but also on its manufacturability [17].

To apply DFM in the Flying-V, especially at the current design stage, not every aspect of manufacturability can be used; a choice is made to include certain manufacturability concepts (section 2.1). The first and most directly related concept is the type of curvature of the OML (section 2.2). The second concept that is addressed in the Flying-V parametrisation is the part variety (section 2.3).

### 2.1. Manufacturability

The concept 'manufacturability' is broken down by Shankar and Jansson into a set of five Core Manufacturability Concepts (CMCs) [2] (Figure 2.1). To take manufacturability into account in the parametrisation of the Flying-V, which is still in the early design stages, the concepts need to be implemented on an abstract level. Detailed designs, material choice, and exact production processes are all still unknown for the Flying-V. *Part variety*, even though the parts themselves are not modelled, is one of the concepts that can be included in the parametrisation by introducing a constant cross-section wing trunk. *Complexity*, is a concept that can be applied at any level of abstraction. With respect to modelling the OML of the Flying-V, the complexity of the shape itself translates into the amount of compound curvature in the shell. *Accessibility* can be improved by getting rid of the part that has a fuselage shell within a wing shell. The fuselage skin can only be accessed from within, and the wing skin can only be accessed from outside. By using the front of the fuselage as the leading edge of the wing, the design becomes less complex and more accessible.

### 2.2. Double curvature

Double curvature, or compound curvature, is one of the cost drivers in aircraft manufacturing. A part that is made of sheet metal that curves in one direction can be created by cutting the metal sheet and bending it into shape [11, 16]. To create double curvature, additional stretching or stamping would be required, which requires more tools and more time and therefore drives up the manufacturing

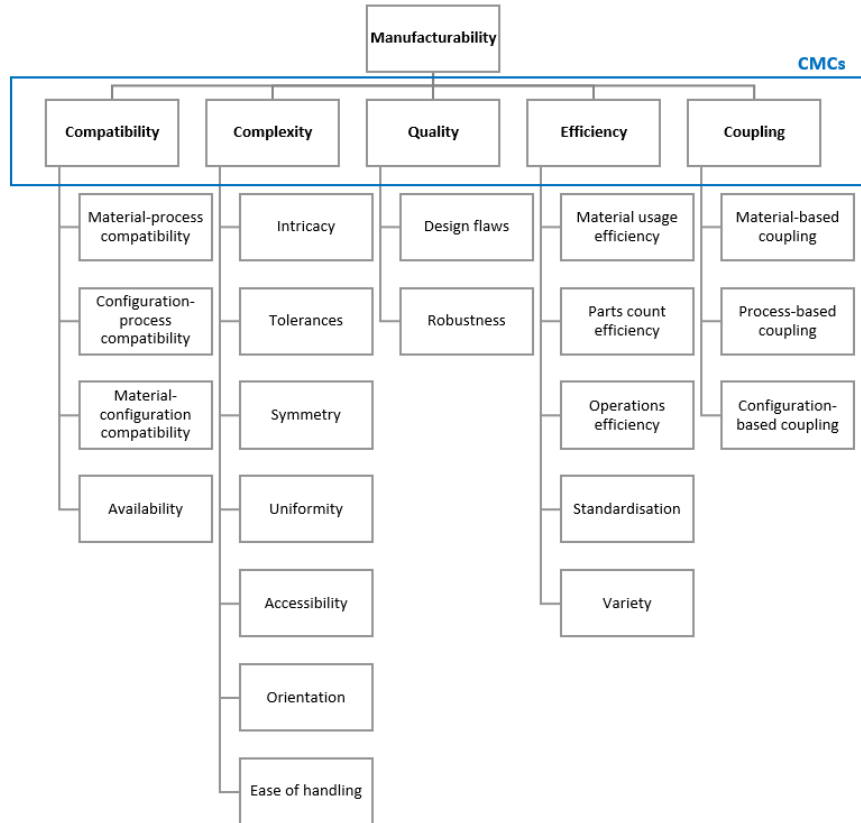


Figure 2.1: Core Manufacturability Concepts [2]

costs. Furthermore, according to Van der Laan and Hootsmans [16], double curvature in sheet metal introduces stresses and could result in local buckling. To prevent this, smaller sheets have to be used, which in addition to increasing manufacturing costs, also increases the weight. In composites, double curvature can cause fiber wrinkling. To prevent this, lay-up tapes should be smaller, which also increases the manufacturing costs.

A developable surface is a surface that has zero double curvature. It is also referred to as a flat-wrap surface. Raymer (2012) [11] explains several ways to loft a flat-wrapped surface. The easiest way is a constant cross-section loft. A loft that uses the same cross-sectional shape, but the size of the section linearly varies, is also a flat-wrapped surface. A drawback of using flat wrap surfaces, is that they are often less desirable from an aerodynamic point of view [11], and therefore in aircraft design a compromise needs to be made between manufacturability and aerodynamic efficiency.

### 2.3. Part variety and part count

Included in the CMC *efficiency* are part count efficiency, and variety. In Design for Manufacturing and Assembly (DFMA), part count reduction is one of the most basic approaches to increase manufacturability [12, 13]. According to Boothroyd (1994) it can achieve the largest improvement in terms of manufacturing cost. The part count is not included in the OML parametrisation strategy because other than the fuselage and the wing, no parts are modelled. Minimising part variety, however, is included in the Flying-V parametrisation. Part variety also relates to the complexity of the design of the assembly. More variety in parts requires more variety in the manufacturing process, which drives up the cost of the product. Also part variety reduction is an objective that conflicts with a major design objective in aircraft design: minimising weight [18].

# 3

## Geometry parametrisation method

A parametrisation of the Flying-V OML in the form of an engineering application allows automatic generation of Flying-V shapes, which is very useful for aerodynamic optimisations. In this research project, the parametrisation is implemented using ParaPy. This requires the use of Object-Oriented Programming (OOP). One of the disciplines in the application is the *geometry*, which is the subject of this chapter.

The main structure of the geometry model is visualised in a class diagram in [Figure 3.1](#). A more elaborate version of this class diagram can be found in [Appendix A](#). Two main components of the Flying-V are the fuselage and the wing. Both fuselage and wing are instances of the class `SymmetricComponent`, which means they both have a starboard part, which is an instance of either `SemiWing` or `SemiCabin`. These last two classes contain the component-specific attributes and parts.

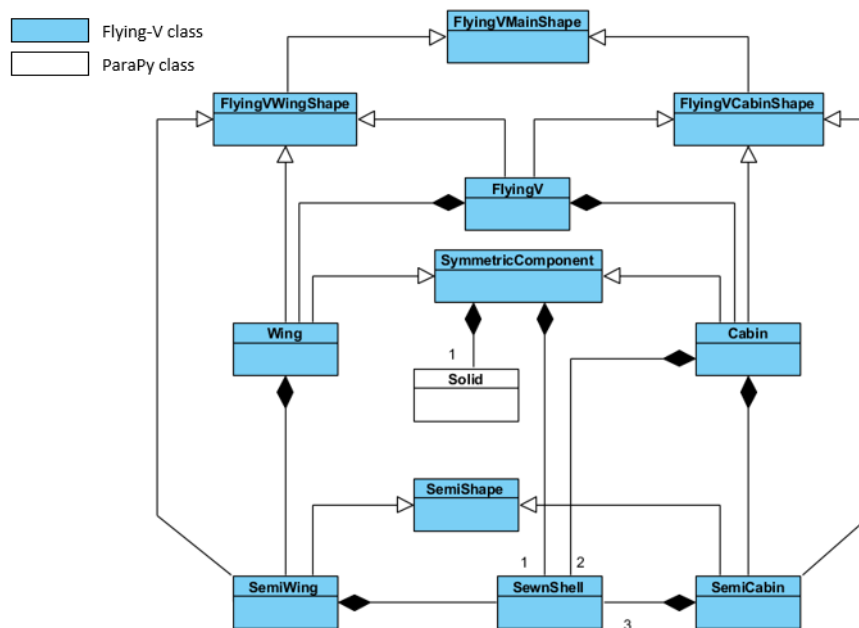


Figure 3.1: UML class diagram of the main Flying-V components

The basic strategy to parametrise the Flying-V geometry is to use lofted surfaces ([section 3.1](#)). The wing is built around the fuselage. Since the reason for existence of any transport aircraft is to transport passengers and cargo, it makes sense to take the fuselage ([section 3.2](#)) as starting point of the parametrisation and to build the aerodynamic shape (wing) around it ([section 3.3](#)). This resulting geometry can be evaluated to determine the reference area of the wing, and the total volume of both the wing and the fuselage ([section 3.4](#))

### 3.1. Lofted surfaces

According to Sóbester and Forrester, the “status quo” parametrisation strategy for a topologically simple three-dimensional body is to view the OML as a “surface lofted over a series of cross-sections generated by parallel cut planes” [14, p. 29]. The parametrisation of the Flying-V is also based on this principle, with the two differences that (1) the sections are not necessarily parallel and that (2) the OML exists of more than one loft. In the context of this thesis, these lofts are called `Trunks` (Figure 3.2). Both the Flying-V OML and fuselage exist of multiple trunks. The

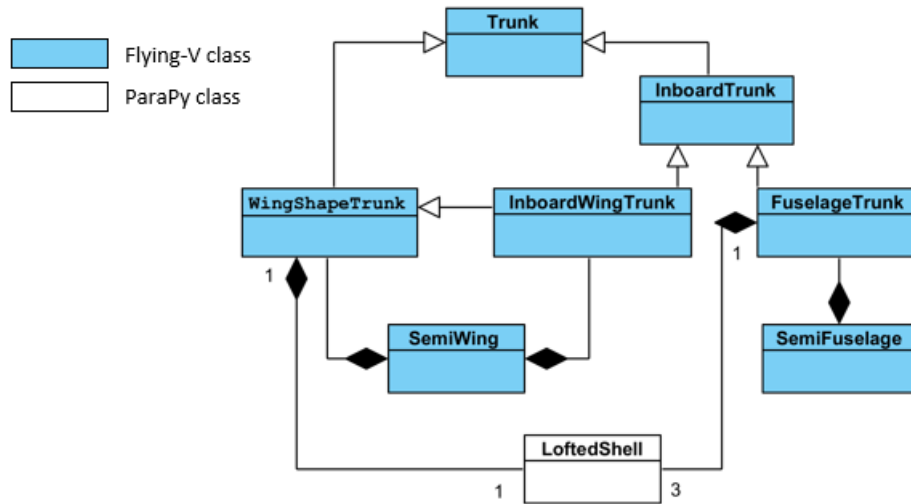


Figure 3.2: UML class diagram of the different trunks

### 3.2. Fuselage

Benad [4] envisioned the fuselage of the Flying-V to have the shape of two oblique circular cylinders that are connected in the middle, to create the V-shape. In his design, fuselage cuts in planes parallel to the symmetry plane are ellipses, and the cross-sections in planes orthogonal to the leading edge are circles. The cross-sectional size of the fuselage would be governed by the circular radius. At TU Delft, the fuselage design changed to have oval, instead of circular, cross-sections [1]. The specific oval that is applied for the fuselage of the Flying-V is that of Hoogreef (2012) [10, 19, 20], which was designed originally for a blended wing body aircraft, with the fuselage’s longitudinal axis aligned with the aircraft’s longitudinal axis. The oval shape provides more design flexibility (4 design variables) than a circle (1 design variable).

In the proposed Flying-V model, the parametrisation of the oval cross-section in the fuselage is slightly different than the previous Flying-V fuselage parametrisation by Faggiano (2016) [5] and therefore also different than the original oval cross-section parametrisation by Hoogreef [10] (3.2.1). The three-dimensional shape of the oval is created using several `FuselageTrunks` (3.2.2).

#### 3.2.1. Fuselage cross-section

The Flying-V fuselage cross-sectional shape is defined by five parameters: the crown height ( $H_1$ ), the cabin height ( $H_2$ ), the keel height ( $H_3$ ), the cabin width at specified height ( $w_H$ ), and the specified height at which the width is defined ( $H_w$ ), (Table 3.1, Figure 3.3). By using the width at a specified height (e.g. the arm-rest height) instead of the floor width, one extra design parameter is introduced to the oval cross-section parametrisation, resulting in five parameters instead of four. Since the floor width and the ceiling width are not necessarily equal, the walls are not exactly vertical but oblique. Therefore, the cabin width is a function of the vertical coordinate. The reason for introducing the extra variable is to provide the designer with the freedom to decide at which height the cabin width should be constrained.

Per definition of this oval concept, the oval consists of four arcs: the crown arc, the keel arc, and two side arcs. The cross-sectional shape is symmetrical with respect to its vertical axis, so the shape

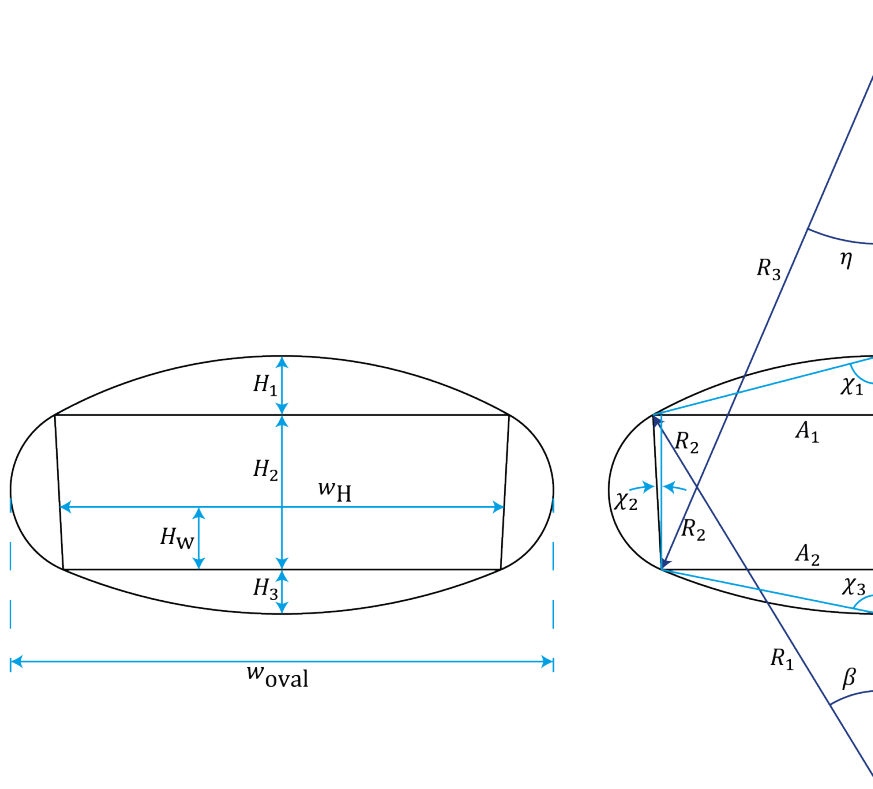


Figure 3.3: Oval fuselage cross-section parametrisation

Table 3.1: Oval fuselage section input parameters

Parameter	Symbol	Unit
Cabin height	$H_2$	m
Cabin width at arm-rest height	$w_{\text{cabin}}$	m
Arm-rest height	$H_{\text{arm}}$	m
Crown height	$H_1$	m
Keel height	$H_3$	m

is defined by three different arcs. At the fuselage nodes, which are the corners of the trapezoid, the two connected arcs are tangent. This tangency condition translates to the following equation [5]:

$$\arctan \chi_1 + \arctan \chi_2 = \arctan \chi_3 \quad (3.1)$$

Because the oblique line is a straight line, :

$$\frac{H_2}{A_1 - A_2} = \frac{H_W}{A_H - A_2} \quad (3.2)$$

which can be rewritten to:

$$A_2 = \frac{H_2 A_H - H_W A_1}{H_2 - H_W} \quad (3.3)$$

These two equations (3.3 and 3.1) can be solved for  $A_1$  and  $A_2$  (or  $w_{\text{ceiling}}$  and  $w_{\text{floor}}$ ). With these widths and the three heights known, the relations presented in Hoogreef (2012) [10] determine the oval shape.

The oval width is as follows:

$$w_{\text{oval}} = w_{\text{floor}} + 2(1 - \sin \eta) R_2 \quad (3.4)$$

### 3.2.2. Fuselage planform

In terms of *fuselage* structural efficiency and manufacturability, a constant cross-section fuselage is preferred to a tapered fuselage because that is closer to a cylinder, which is structurally a suitable shape for a slender pressure vessel [14]. In terms of *wing* structural efficiency and aerodynamic efficiency, a tapered wing is preferred [14]. Contrary to conventional tube-and-wing aircraft, the wing shape of the Flying-V is governed by the fuselage and vice versa, because the fuselage is part of the wing. As such, the fuselage and wing have conflicting requirements. In addition, one of the requirements outlined in section 1.1 is that part of the fuselage should have a constant cross-section, to simplify shrinking and shortening of the wing for a family of Flying-V's. The proposed fuselage (Figure 3.4) has a constant cross-section trunk that is trimmed at the symmetry plane. The outboard part of the fuselage has a linearly varying cross-section, which allows that fuselage trunk to be tapered. To keep the leading-edge sweep constant for the whole inner wing, this outboard trunk is rotated with respect to the inboard trunk around an axis parallel to the aircraft's top axis. This requires a transition piece between these two fuselage segments. There are two different oval profiles used to create the lofts. The profiles for the constant cross-section trunk and the connection trunk are equal. The tapered trunk is a loft between two different profiles.

The transition trunk is created by revolving an oval around an axis that is parallel to the aircraft's top axis and located at the leading edge point between the inboard fuselage trunk and the outboard fuselage trunk. The angle that this cross-section is revolved to create the trunk is  $\mu$  (Equation 3.5, Figure 3.5). The result is a toroidal, and thus doubly curved, shell. The revolved shapes of the individual arcs are tori. Schmidt (2013) first used the oval fuselage in a toroidal shape [20]. The loft at the leading edge is part of a horn torus (i.e. its major radius is equal to its minor radius). In terms of pressurisation this is an interesting trunk. In the inner half of a torus, the pressurisation loads are higher than in a cylinder, and in the outer half of a torus, the pressurisation loads are lower than in a cylinder [20].

$$\mu = \arctan \frac{w_{\text{oval}_1} - w_{\text{oval}_3}}{2L_3} \quad (3.5)$$

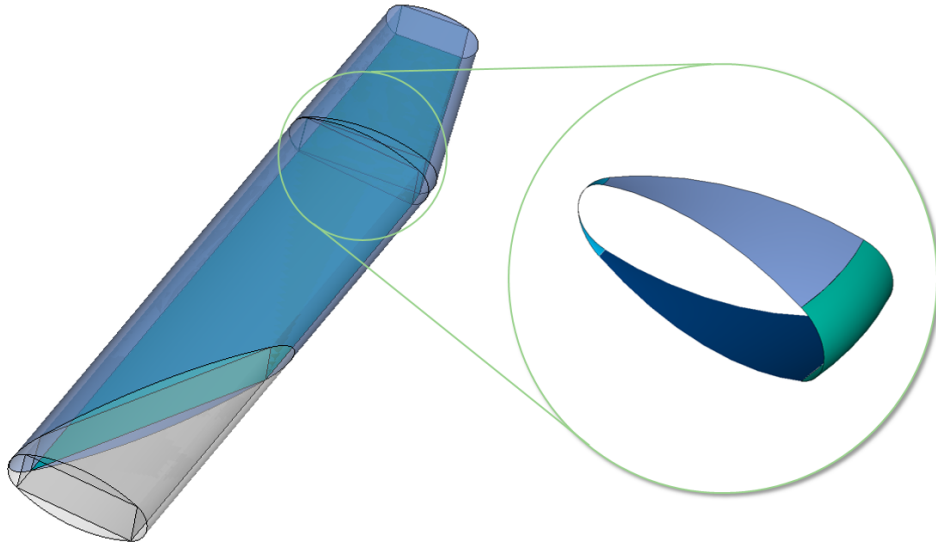


Figure 3.4: three-dimensional visualisation of a semi fuselage

The parameters that define the size of the cabin in terms of planform are the lengths of the cabin trunks, the arm-rest height of the oval of the inboard trunk, and the width of the most outboard oval cross-section (Table 3.2). The cabin loft geometries are created using the class `OvalFuselageTrunk`, which has three `LoftedSurfaces`: for the oval, the trapezoid, and for the floor.

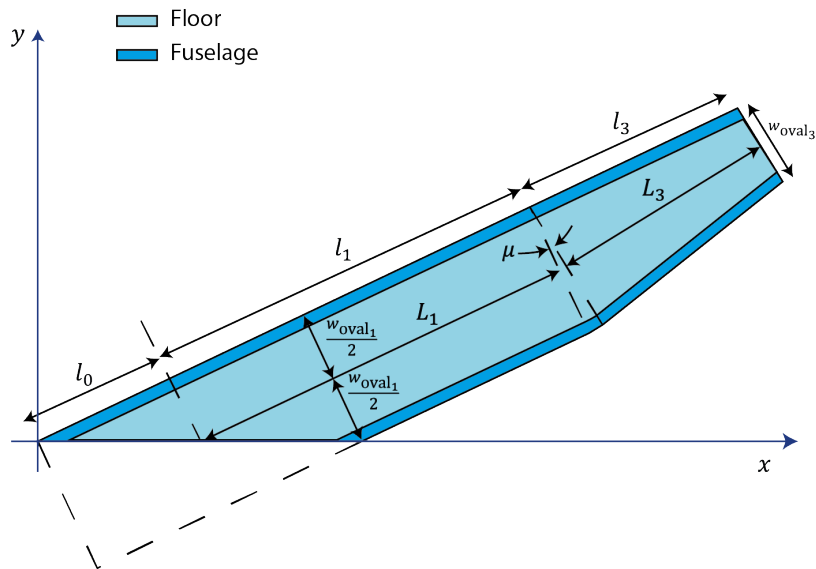


Figure 3.5: Fuselage planform parameters

Table 3.2: Fuselage planform input parameters

Parameter	Symbol	Unit
Untapered fuselage length (centre line length)	$L_1$	m
Tapered fuselage length (centre line length)	$L_3$	m
Width at input height of section 1	$w_{H_1}$	m
Width at input height of section 3	$w_{H_3}$	m

### 3.3. Wing

The positions of the profiles that form the inboard wing lofts are the same as those that form the fuselage lofts. The reason for this is that at these positions structural frames are expected to be present, and the ribs of the rear wing are located in the same planes as the fuselage frames [1]. Therefore, the loft profiles of the rear wing and the fuselage are also constructed in the same planes. In the engineering application this means that the oval fuselage section is an input for the inboard aerofoil (subsection 3.3.1). The outboard wing uses the Class function/Shape function Transformation (CST) method for curve parametrisation of Kulfan (2008) [21], which was also used by Faggiano to parametrise the outboard aerofoils in his model (subsection 3.3.2). The  $x$ - and  $y$ - positions of the wing sections are combined in the planform (subsection 3.3.3). The  $z$  position of the sections is defined by the dihedral and the orientation in the aerofoils'  $xz$  plane is determined by its incidence angle (subsection 3.3.4).

Figure 3.6 shows the structure of the programme that models the wing of the Flying-V. Since the wing is symmetric, only a semi-wing needs to be modelled. The resulting wing shape is a combination of that semi-wing and its mirrored counterpart. Because the shape of the aerofoil will depend on the shape of the oval fuselage, the cross-section of the oval fuselage (so an `OvalFuselageSection` object) is an input for the `InboardAerofoil` class.

#### 3.3.1. Inboard aerofoil: an oval fuselage cross-section extended with a rear aerofoil

The inboard aerofoils are constructed around the fuselage. The approach is based on that of Faggiano. The major difference between this proposed aerofoil parametrisation and Faggiano's is that he created the aerofoil lofts in planes that are parallel to the aircraft's symmetry plane (butt planes), whereas the parametrisation proposed here creates inboard aerofoil lofts in planes that are orthogonal to the fuselage's centreline.

The oval section is the basis of the inboard aerofoil shape (Figure 3.7). The class that represents

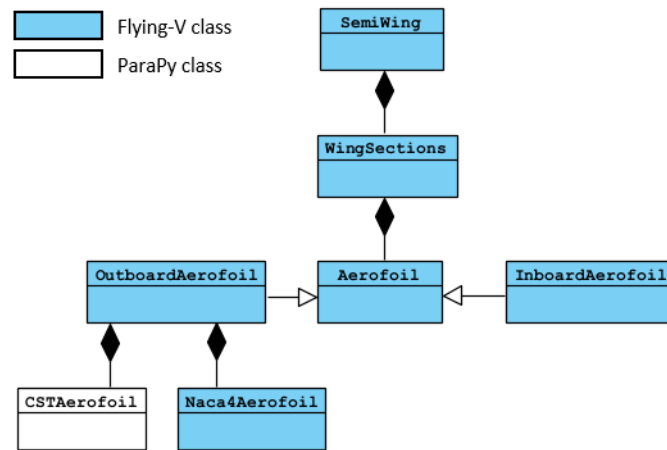
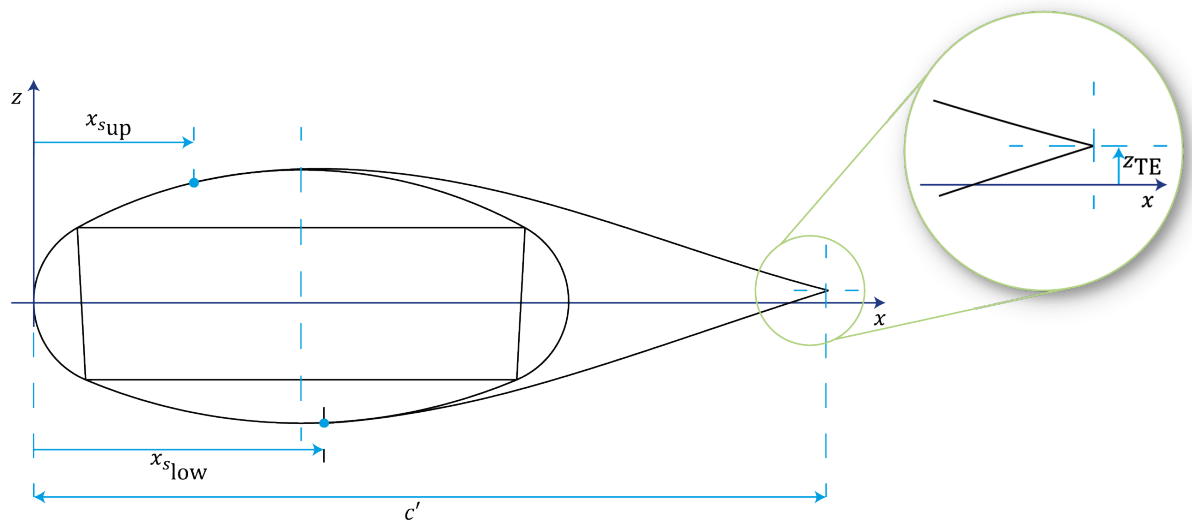


Figure 3.6: UML class diagram of the wing component

this shape is the `InboardAerofoil` class. Two curves define the rear wing; an upper- and a lower curve. They join the oval curve at locations determined by the parameters  $\bar{x}_{sup}$  and  $\bar{x}_{low}$  (Equation 3.6). This introduces an extra input parameter; in the former parametrisation of Faggiano these were equal.

$$\bar{x}_s = \frac{x_s}{W_{oval}} \quad (3.6)$$

The rear wing curves join each other at the trailing edge, which location is determined by the input

Figure 3.7: Inboard aerofoil drawing in its own  $xz$  plane

parameters  $c'$  and  $z_{TE}$ . Each of these curves is a fourth-order polynomial. There are four conditions that the polynomial has to satisfy:

- Pass through trailing edge point
- Pass through start point
- Tangency at start point
- Curvature continuity at start point

Translating these conditions to the polynomial results in the following set of equations for one fairing curve:

$$\begin{aligned}
 x_{\text{end}}^3 a_1 + x_{\text{end}}^2 a_2 + x_{\text{end}} a_3 + a_4 &= z_{\text{end}} & -c x_{\text{end}}^4 \\
 x_{\text{start}}^3 a_1 + x_{\text{start}}^2 a_2 + x_{\text{start}} a_3 + a_4 &= z_{\text{start}} & -c x_{\text{start}}^4 \\
 3x_{\text{start}}^2 a_1 + 2x_{\text{start}} a_2 + a_3 &= \frac{dz}{dx}(x_{\text{start}}) & -4c x_{\text{start}}^3 \\
 6x_{\text{start}} a_1 + a_2 &= \frac{d^2z}{dx^2}(x_{\text{start}}) & -12c x_{\text{start}}
 \end{aligned}$$

where  $c$  is the polynomial coefficient that is used as input parameter. The only unknowns are the four  $a_i$  coefficients, which can be determined by solving this system of four equations. All geometrical input parameters of the `InboardAerofoil` class are summarised in [Table 3.3](#).

Table 3.3: Inboard aerofoil parameters

Parameter	Symbol	Unit
Planform chord, normalised	$\bar{c}$	m
Vertical position of trailing edge	$z_{\text{TE}}$	m
Upper curve coefficient	$c_{\text{up}}$	$\text{m}^{-3}$
Lower curve coefficient	$c_{\text{low}}$	$\text{m}^{-3}$
Upper curve starting location	$\bar{x}_{\text{sup}}$	-
Lower curve starting location	$\bar{x}_{\text{slo}}$	-

### 3.3.2. Wing outboard aerofoils

To parametrise the aerofoil profiles that are not restricted by the oval shape, the CST method of Kulfan [21] is employed. This is a useful way to parametrise an aerofoil curve with a relatively small amount of parameters, compared to using point coordinates, while still providing design flexibility. The equation for a curve using the CST method is:

$$\zeta(\psi) = C_{N_2}^{N_1}(\psi)S(\psi) + \psi\zeta_T \quad (3.7)$$

where  $\zeta = \frac{z}{c}$ ,  $\psi = \frac{x}{c}$ , and  $\zeta_T = \frac{\Delta z_{\text{TE}}}{c}$ . The class function  $C$ , defined by two parameters  $N_1$  and  $N_2$ , governs the characteristic shape of the curve. The class function is defined as:

$$C_{N_2}^{N_1}(\psi) = \psi^{N_1} [1 - \psi]^{N_2} \quad (3.8)$$

The shape function  $S\left(\frac{x}{c}\right)$  is able to make small changes to the basic curve defined by the clas function. In other words, it can alter the thickness distribution and camber while maintaining the basic shape of the class function. In the Flying-V parametrisation, the parameters of the class function are set to  $N_1 = 0.5$  and  $N_2 = 1.0$ , which ensure a typical NACA aerofoil shape (i.e. with a round nose and a sharp trailing edge). The shape function is a series of Bernstein polynomials multiplied by scaling factors. These scaling factors, or Bernstein coefficients, define the deviation of the basic shape.

The class `OutboardAerofoil` has the possibility to create an aerofoil using the CST method, for which the Bernstein coefficients have to be specified. This class also has the possibility to create a National Advisory Committee for Aeronautics (NACA) 4 digit aerofoil. The CST parametrisation method provides more design flexibility than the NACA 4 digits. Still, for a user who wishes to manually and intuitively create or alter one of the outboard aerofoils, the possibility to use the NACA 4 parametrisation is provided. In the engineering application, these input slots ([Table 3.4](#)) accept either a list of Bernstein coefficients (in which case the CST parametrisation is applied) or a string with four NACA digits (in which case the NACA 4 digit parametrisation is applied).

### 3.3.3. Wing planform

The wing planform parametrisation is shown in [Figure 3.8](#). Because a semi-fuselage consists of three fuselage trunks, a semi-wing has three wing trunks that contain the fuselage. For a given fuselage

Table 3.4: Outboard aerofoil parameters

Parameter	Symbol
Section 4 parameters	$\mathbf{A}_4$
Tip section parameters	$\mathbf{A}_{tip}$

length,  $L_4$  determines the location of the leading edge kink.  $L_4$  is the length that would have to be added to  $L_3$  to have the tapered fuselage continue until its planform leading edge is on the leading edge kink. The choice for this input variable is because from an inside-out design approach point of view this parameter is expected to best facilitate the design of a fuel tank geometry that can be an extension of the fuselage.

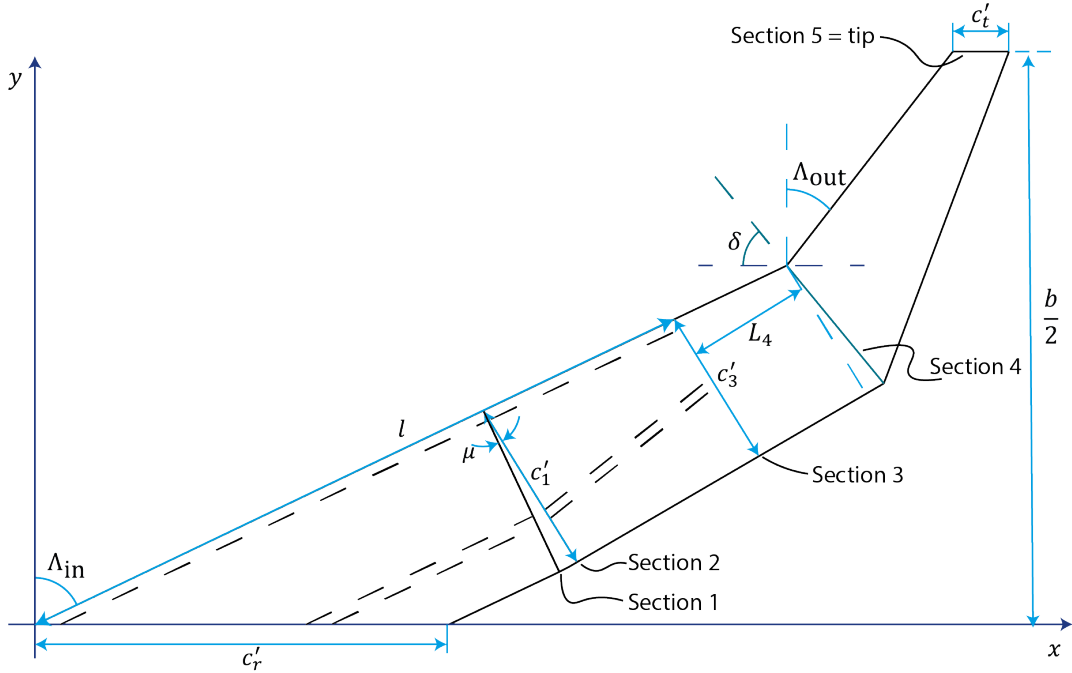


Figure 3.8: (semi-) Wing planform parametrisation

The tip section chord is defined by the overall taper ratio,  $\lambda$ , and its spanwise position is determined by the span,  $b$ . The orientation of section 4 depends on the angle  $\delta$ . A large value for  $\delta$  creates a longer trailing edge for the outboard wing and, therefore, more space for the control surfaces. However, this positions the profile more perpendicular to the free-stream direction. The parametrisation uses linear lofts that are 'sewn' together and therefore, the OML is not smooth at these profile locations. A more perpendicular orientation of the profile can be disadvantageous for the pressure distribution around the wing, because it causes the flow to experience a sharper change in curvature compared to when the section is placed along the free-stream direction.

The wing planform input parameters are listed in Table 3.5. The actual input parameter used to define the chord length of section 1 and 3 is a normalised version of  $c'$  (Equation 3.9). This normalisation simplifies the application of a lower bound for the design variable, which is simply 1 (i.e. the chord length cannot be smaller than the sum of the fuselage input width and the fuselage height at that section).

$$\bar{c}' = \frac{c'}{w_H + H_2} \quad (3.9)$$

For the length  $L_4$  a normalisation is also applied, to deal with the upper bound for this parameter. The upper bound for this variable is when it causes the leading edge of section 4 to reach the wing tip. The

maximum value for  $L_4$  is therefore:

$$L_{4_{\max}} = \left( \frac{b}{2 \cos \Lambda_{\text{in}}} - l \right) \cos \mu \tag{3.10}$$

The normalised input parameter to change this length is:

$$\bar{L}_4 = \frac{L_4}{L_{4_{\max}}} \tag{3.11}$$

Its upper bound is 1 ( $L_4 = L_{4_{\max}}$ )

Table 3.5: Wing planform parameters

Parameter	Symbol	Unit
Span	$b$	m
Planform chord of section 1	$\bar{c}'_1$	-
Leading edge sweep of inboard wing	$\Lambda_{\text{in}}$	°
Leading edge sweep of outboard wing	$\Lambda_{\text{out}}$	°
Taper ratio $\frac{c_r}{c_t}$	$\lambda$	-
Virtual fuselage extension length to leading edge kink	$\bar{L}_4$	-
Planform chord of section 3	$\bar{c}'_3$	-
Orientation angle of section 4	$\delta$	°

### Trailing edge

The trailing edge has four different sweep angles (Figure 3.9). The trailing edge sweep of the most inboard wing trunk is the same as the leading edge sweep, because it has a constant cross-section. The trailing edge of the connection trunk is an arc, because that trunk is toroidal. The trailing edge of trunk 3 and trunk 4 is straight, and these two trunks have the same trailing edge sweep.

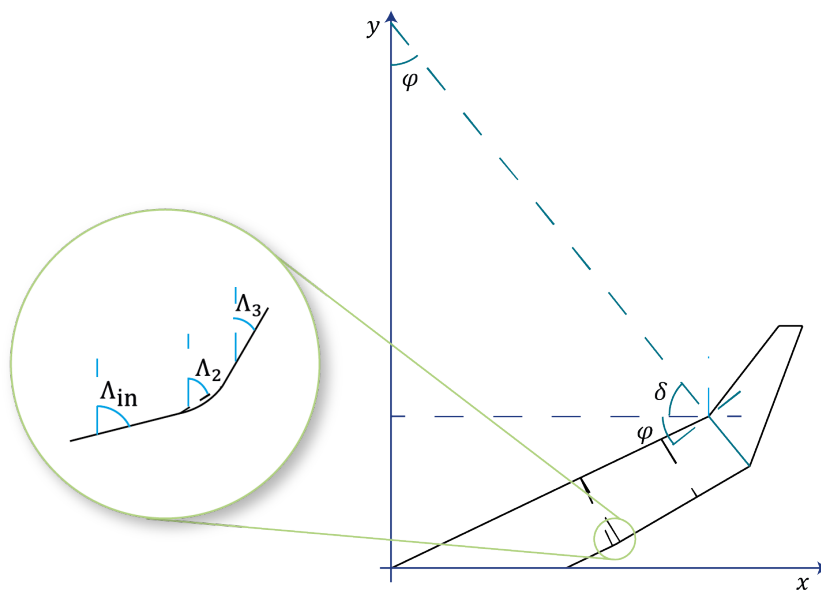


Figure 3.9: Wing planform angles

$$c'_r = \frac{c'_1}{\cos \Lambda_{\text{LEin}}} \tag{3.12}$$

The (projection of the) trailing edge curve in the  $xy$  plane can be approximated by a piecewise continuous linear function:

$$x(y) = c'_r + \begin{cases} y \tan \Lambda_{\text{in}} & \text{if } 0 \leq y \leq y_{\text{TE}_1} \\ (y - y_{\text{TE}_1}) \tan \Lambda_2 + y_{\text{TE}_1} \tan \Lambda_{\text{in}} & \text{if } y_{\text{TE}_1} < y \leq y_{\text{TE}_2} \\ (y - y_{\text{TE}_2}) \tan \Lambda_3 + y_{\text{TE}_1} \tan \Lambda_{\text{in}} + (y_{\text{TE}_2} - y_{\text{TE}_1}) \tan \Lambda_2 & \text{if } y_{\text{TE}_2} < y \leq y_{\text{TE}_4} \end{cases} \quad (3.13)$$

where  $y_{\text{TE}_i}$  is the spanwise location of section  $i$  (see Figure 3.8 for the section numbering). The ( $xy$  plane projected)  $x$  axis of section 4 is described in the aircraft's axis system with the following equation:

$$x(y) = (y_{\text{LE}_4} - y) \tan \varphi + y_{\text{LE}_4} \tan \Lambda_{\text{in}} \quad (3.14)$$

Setting equation 3.13 equal to equation 3.14 results in the  $x$  and  $y$  locations of the trailing edge of section 4:

$$x_{\text{offset}} = y_{\text{TE}_1} (\tan \Lambda_{\text{in}} - \tan \Lambda_2) + y_{\text{TE}_2} (\tan \Lambda_2 - \tan \Lambda_3) + c'_r \quad (3.15)$$

$$y_{\text{TE}_4} = \frac{y_{\text{LE}_4} (\tan \Lambda_{\text{in}} + \tan \varphi) - x_{\text{offset}}}{\tan \Lambda_3 + \tan \varphi}$$

$$x_{\text{TE}_4} = y_{\text{LE}_4} \tan \Lambda_2 + x_{\text{offset}}$$

$$c_4 = \frac{x_{\text{TE}_1} - x_{\text{LE}_2}}{\sin \varphi} \quad (3.16)$$

### 3.3.4. Twist and dihedral

Not only the aerofoil shapes, but also the dihedral and twist angles control the shapes of the wing trunks that are not built around the fuselage (Table 3.6). Geometric twist is the change in angle of incidence of the aerofoils along the span, usually measured with respect to the root aerofoil [11]. Wing twist is used to prevent tip stall and to shape the lift distribution to be more elliptical. In the Flying-V, the wing twist is controlled by the incidence angle of the two sections that define the outboard wing and by the vertical location of the trailing edge of the inboard wing sections.

The parametrisation also allows for dihedral to be added. The wing trunks that are built around the fuselage do not have a dihedral parameter, because these are restricted by the presence of the fuselage. The dihedral angle of trunk 4 and 5 is the angle of its leading edge and the horizontal aircraft's  $xy$  plane:

$$\Delta z_i = z_i - z_{i-1} = l_i \tan \Gamma_i \quad (3.17)$$

where  $i$  is the index that denotes the wing trunk number.

Table 3.6: Outboard aerofoil parameters

Parameter	Symbol	Unit
Dihedral of trunk 4	$\Gamma_4$	°
Dihedral of trunk 5	$\Gamma_5$	°
Incidence angle of section 4	$i$	°
Incidence angle of section tip	$i$	°

## 3.4. Geometry evaluation

Next to the Flying-V fuselage and OML shapes themselves, some properties are useful for further analysis. These are computed by the `Wing` class. The wing area and Mean Aerodynamic Chord (MAC) are generally used to compute aerodynamic coefficients. The volumes of the fuselage and wing indicate how much space is left for other purposes, such as placing fuel tanks.

The Flying-V wing area is calculated by integrating the chord length along the aircraft's lateral axis (Equation 3.18). This integration is performed numerically, using a composite Simpson's rule [22], by

creating a number of streamwise wing cuts along the semi span and determining their chord lengths. The number of cuts can be specified as an input parameter.

$$S = \int_{-\frac{b}{2}}^{\frac{b}{2}} c(y)dy = 2 \int_0^{\frac{b}{2}} c(y)dy \quad (3.18)$$

The aerofoil chord,  $c$ , is the straight line between the trailing edge and the leading edge, where the leading edge is the point on the aerofoil curve furthest away from the trailing edge. Faggiano used the planform area as the reference area. If small incidence angles are assumed for the streamwise aerofoils, the aerofoil chord is approximately equal to the planform chord, and the planform wing area is approximately equal to the wing area.

The MAC is calculated using the following integral [23]:

$$\text{MAC} = \frac{2}{S} \int_0^{\frac{b}{2}} c^2(y)dy \quad (3.19)$$

This is approximated in the code by Simpson's rule.

The volume of the fuselage and the OML is computed by using the same streamwise cuts as for the reference area. The cross-sectional area,  $A(y)$  of the cuts is integrated along the (semi-) span to obtain the volume:

$$V = 2 \int_0^{y_{\max}} A(y)dy \quad (3.20)$$

where the maximum  $y$  value of the object is the most outboard sample point of the most outboard edge of the shell. Sample points are a built-in attribute of the ParaPy class `Edge`. This integral is also approximated by numerical integration, using Simpson's rule. The area  $A(y)$  is determined by intersecting the shell with a butt plane that is located at  $y$ , using that intersection to create a face, and retrieving the area of that face. The ParaPy class `Face` has a built in attribute that represents its area. This method to determine the volume of the fuselage or wing is a bit cumbersome, because the ParaPy class `Solid` has an attribute to determine the volume of a solid (which can be created using a closed shell). However, this did not provide reasonable numbers for the Flying-V volume. The sum of the volumes for each individual wing trunk were not equal to the volume of the `SewnShell` (the wing trunks sewn together).

The volume computation is an attribute of the Flying-V class `SemiShape`, which is the parent class of both `SemiWing` and `SemiCabin`.



# 4

## Aerodynamic analysis method

Part of the research objective is that the parametrisation can be used in an aerodynamic design optimisation. A typical aerodynamic optimisation objective is to maximise the lift-to-drag ratio, which is a function of the design vector  $\mathbf{x}$  (Equation 4.1). Many geometrical input parameters that are described in chapter 3 are intended as design variables for an aerodynamic optimisation of the Flying-V OML.

$$f(\mathbf{x}) = \frac{C_L}{C_D} \quad (4.1)$$

The aerodynamic analysis of the Flying-V shape proposed in this thesis is similar to that of Faggiano [5]. Because optimisation requires many objective function evaluations, the evaluation of the objective function should not be too costly in terms of computational time. Therefore the aerodynamic analysis of the aircraft in cruise conditions is based on Euler equations. Euler equations are a simplification of the Navier-Stokes equations by assuming inviscid flow [24]. The computational tool that is used to analyse the Euler equations is SU2 (section 4.1). This is an open source software package capable of carrying out high fidelity Partial Differential Equation (PDE) analysis [25]. Because the Euler equations neglect viscosity, an additional empirical module is employed to estimate the drag contribution of viscous effects (section 4.2). The inviscid drag coefficient (by SU2) and the viscous drag coefficient (by the empirical module) are added to determine the drag coefficient (Equation 4.2).

$$C_D = C_{D_{inv}} + C_{D_{visc}} \quad (4.2)$$

The viscous drag contribution is approximated by semi-empirical relations presented by Torenbeek (1982) [26] and Raymer (2012) [11]. The class diagram of the aerodynamic analysis module is shown in Figure 4.1, which shows that both the classes `ViscousApproximations` and the `SU2` are parts of the `AerodynamicAnalysis`.

### 4.1. Euler analysis

One of the main parts of the aerodynamic analysis module is the `SU` class, which activates the external aerodynamic solver, SU2, to carry out an Euler analysis. The Euler equations can be derived from the Navier-Stokes equations by ignoring viscosity effects and by assuming a steady flow [11]. For transonic flow simulations the Reynolds number is high and viscous and turbulence effects are relatively small [27], provided the flow is attached. These flows can be modelled using the Euler equations. The flow around the Flying-V in cruise conditions is simulated by analysing the Euler equations, using the SU2 tool. The proposed SU2 implementation can be improved in the future to include the capability to use other (viscous) flow equations, such as Reynolds-averaged Navier Stokes (RANS). For this research, however, implementing such a simulation is out of scope. Viscous simulation requires refinement of the grid near the walls to resolve the boundary layer, and it requires the use of turbulence models.

To run an SU2 simulation, two input files are required: a mesh file (subsection 4.1.1) that contains the element connectivity information, and a configuration file that contains the SU2 settings (subsection 4.1.2). The SU2 analysis is verified using the results of Faggiano (subsection 4.1.3).

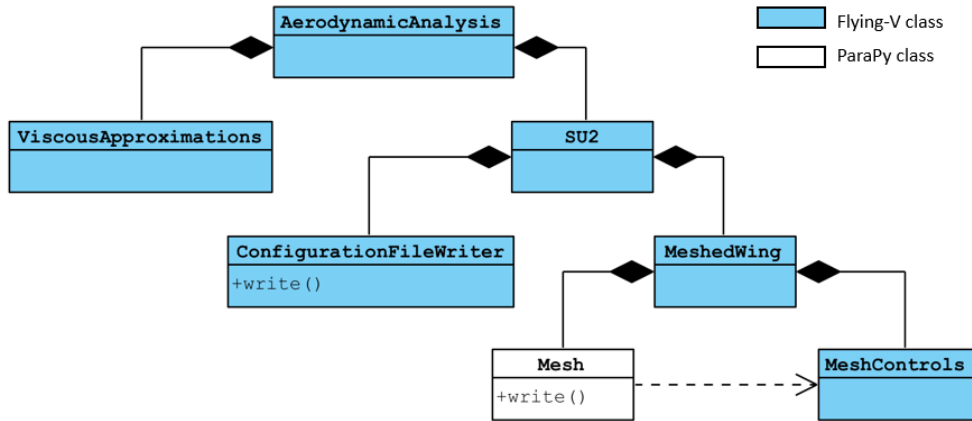


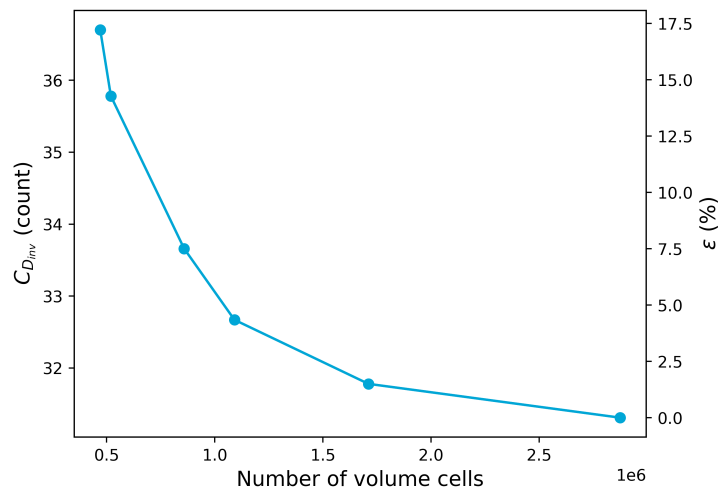
Figure 4.1: UML class diagram of the aerodynamic analysis module

#### 4.1.1.1. Mesh

For the SU2 simulation, an unstructured grid is generated using the ParaPy mesh library. Although an unstructured mesh is computationally less efficient and accurate compared to a well designed structured mesh, the advantage of an unstructured grid is that it can arbitrarily be applied to a complex shape. The mesh algorithms are implemented in the Salome package in ParaPy. The class `MeshedWing` contains two parts: the mesh itself, and the mesh controls (Figure 4.1). The mesh itself is an instance of the ParaPy class `Mesh` and the mesh controls is an instance of the class `MeshControls`. The parameters that control the mesh fineness are the same as those of the Flying-V parametrisation of Faggiano. Because the new parametrisation has a different topology, a new grid convergence study is performed to verify that the default mesh control settings that were presented by Faggiano are still sufficient. The inputs for the Flying-V shape used for the grid convergence study are listed in Appendix B, Table B.1. The results of the mesh convergence study are shown in Figure 4.2. The quantity  $\epsilon$  is the relative difference between the drag coefficients computed by the tested mesh and the finest mesh that is tested (Equation 4.3).

$$\epsilon = \frac{C_{D_{inv}} - C_{D_{inv}}^{fine}}{C_{D_{inv}}^{fine}} \quad (4.3)$$

The drag coefficient of the mesh with 1.7 million cells is 1.5 % higher than the drag coefficient of the

Figure 4.2: Inviscid drag coefficient for different mesh refinements,  $M = 0.85$ ,  $C_L = 0.266$

finest tested mesh. This mesh is chosen as the default mesh, and its mesh control parameters are listed in [Table 4.1](#). The parameters that control the mesh fineness are the same as those implemented by Faggiano (2016) [5]. An example of a coarse grid is shown in [Figure 4.3](#). This visualisation shows that near the root, tip, leading edge, and trailing edge, the mesh density is relatively high. This is because the mesh controls of these edges are controlled by the same parameter, *the nodes per length* parameter. The intermediate edges of the profiles have less density in this figure. These are controlled by a different parameter, *the max size wing* parameter.

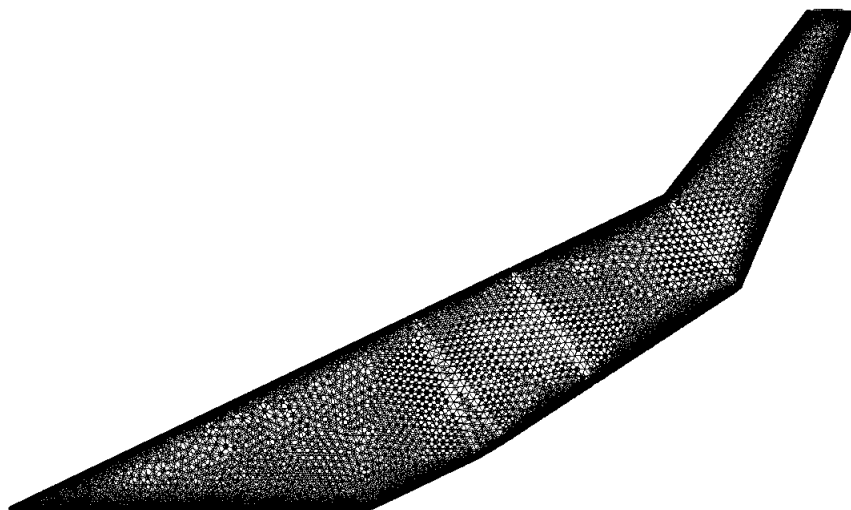


Figure 4.3: An example of a coarse surface grid (not the default grid)

Table 4.1: Default grid controlling parameters

Parameter	Controls elements on	Default value
Nodes per length	Leading edge, trailing edge, tip, and root section	15
Max size wing	Wing faces, section 1, 2, 3, and 4	0.1
Outer domain maxim	Outer domain faces	15.0
Triangular element growth rate	Faces	0.1
Tetrahedral maximum size	Volume	15.0
Tetrahedral growth rate	Volume	0.3

The mesh controlling parameters used for the grid convergence study are shown in [Appendix C](#).

There is the possibility to parametrise the connection trunk differently than explained in [subsection 3.2.2](#), to improve meshing. The toroidal trunk's leading edge practically has zero length and because of that, the aspect ratio of the elements near the leading edge of that trunk becomes very high. The alternative parametrisation allows a leading edge length to be specified for this connection trunk. To realise this without curving the leading edge, the trunk becomes a linear loft between the outboard profile of the untapered trunk and the inboard profile of the tapered trunk.

#### 4.1.2. Configuration

The configuration file contains the SU2 settings, such as the type of flow equations, solver, boundary conditions, and convergence criteria. The configuration file template that is used for this research is based on an example provided with the SU2 software, which is the analysis of an Onera M6 wing in inviscid flow. The boundary conditions of the SU2 analysis are ([Figure 4.4](#)):

- Free-stream conditions for the outer domain faces
- Euler wall for the Flying-V surface

- Symmetry for the symmetry plane

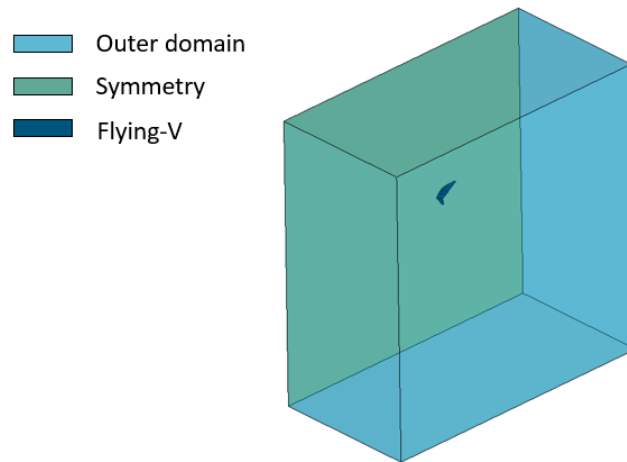


Figure 4.4: Boundaries of the computational domain

#### 4.1.3. Verification

The case to test the SU2 aerodynamic analysis is to use the mesh file of Faggiano (2016) [5] and run SU2 using a new configuration file. The proposed parametrisation employs SU2 version 7, while Faggiano used SU2 version 4. The configuration file inputs have changed in the mean time. The exact same aerodynamic coefficients are not reproduced by the new SU2 analysis module (Table 4.2), but the pressure contours over the wing appear to be very similar (Figure 4.5).

Table 4.2: Coefficients of two SU2 version results with the current Flying-V design's geometry

	SU2 version 4	SU2 version 7	Change
$C_L$	0.1330	0.1328	- 0.19 %
$C_{D_{inv}}$ (counts)	27.24	25.58	- 6.08 %

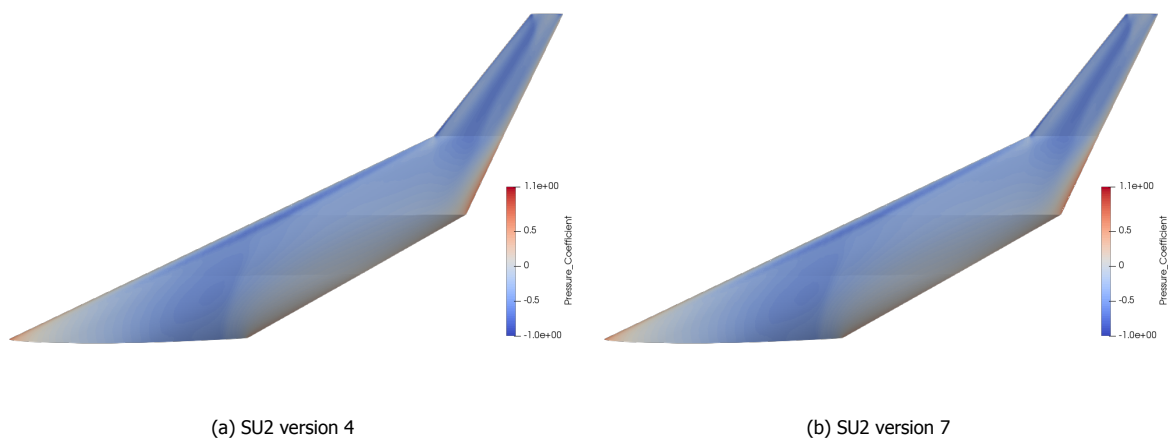


Figure 4.5: Pressure coefficient contour plots over the top surface of the current Flying-V geometry

## 4.2. Viscous drag estimation

The calculation of the viscous drag coefficient of the Flying-V uses that of the flat plate analogy, as explained by Torenbeek (1982) [26]. The implementation requires a form factor to be determined, which is a geometrical property (4.2.1). Combining the form factor with the skin friction coefficient, which depends on the flight conditions, results in the viscous drag coefficient (4.2.2). Because these are semi-empirical relations, mainly based on conventional shapes, the validity is limited (subsection 4.2.3). The viscous drag calculations are part of the class `ViscousApproximations`.

### 4.2.1. Form factor

The form factor is a quantity required for the viscous drag estimation, and it is a geometrical property of the wing OML (Equation 4.4). The wing is divided into strips, and the form factor is determined per strip.

$$ff = 1 + \varphi \cos^2 \Lambda_{\frac{1}{2}} \quad (4.4)$$

The shape correction factor,  $\varphi$ , accounts for the difference between a flat plate and the body's shape. It can be approximated by the following relation for aerofoils with a thickness to chord ratio of maximum 21%:

$$\varphi = 2.7 \frac{t}{c} + 100 \left( \frac{t}{c} \right)^4 \quad (4.5)$$

The thickness to chord ratio,  $\frac{t}{c}$ , is determined by using the average thickness and the average chord of the strip.

### 4.2.2. Viscous drag

The profile drag is defined by Torenbeek [26, p. 490] as "drag due to the boundary layer and regions of separated flow around the main airplane parts placed in isolation". The boundary layer, and flow separation are both viscous phenomena and therefore, the term *profile drag* is equivalent to the term viscous drag in this thesis. At small angles of attack, for well-streamlined, smooth aircraft components, the skin friction drag is the primary part of the profile drag. Based on strip theory, assuming no spanwise interaction, the profile drag for a three-dimensional wing is [26]:

$$C_{D_p} = \frac{2}{S} \int_0^{\frac{b}{2}} c_{d_p} c \, dy \quad (4.6)$$

This coefficient can be split for the purpose of drag estimation as:

$$c_{d_p} = c_{d_{p_{\min}}} + dc_d(c_l) \quad (4.7)$$

For a section of a 3-dimensional wing, the minimum section profile drag coefficient includes a correction for the sweepback angle, which is included in the form factor  $ff$ :

$$c_{d_{p_{\min}}} = 2C_F ff \quad (4.8)$$

where  $C_F$  is the flat plate skin friction coefficient. The factor 2 in this equation is because the friction drag coefficient is based on two sides of the aerofoil being exposed to the flow. This friction coefficient for a fully turbulent boundary layer [11] is a function of the local Reynolds number and the Mach number (Equation 4.9). If the surface is rough, the friction coefficient is higher and in that case the Reynolds number that is used in this equation is replaced by a fictitious Reynolds cutoff number to increase the friction coefficient (Equation 4.10, Equation 4.11).

$$C_F = \frac{0.455}{(\log_{10} Re^*)^{2.58} (1 + 0.144 Ma^2)^{0.65}} \quad (4.9)$$

$$Re_{\text{cutoff}} = 44.62 \left( \frac{l}{k} \right)^{1.053} Ma^{1.16} \quad (4.10)$$

$$Re^* = \min(Re, Re_{\text{cutoff}}) \quad (4.11)$$

The viscous drag is calculated at cruise conditions. Assuming that the aircraft cruises at its minimum drag coefficient, the second term of Equation 4.7 can be neglected, so that:

$$c_{d_p} = c_{d_{p_{\min}}}$$

So, from Equation 4.6, the drag area becomes:

$$C_{D_p} S = 2 \int_0^{\frac{b}{2}} c_{d_{p_{\min}}} c dy \quad (4.12)$$

$$= 2 \int_0^{\frac{b}{2}} 2C_{F_i} ff c dy \quad (4.13)$$

The factor 2 combined with the chord length is an approximation for the wetted area. Since the wetted area of a Flying-V strip can be calculated, this approximation can be refined ( $S_{\text{wet}} \approx 2c dy$ ). The integral is numerically computed with the following equation:

$$C_{D_p} \approx \frac{2}{S} \sum_{i=0}^n C_{F_i} ff_i S_{\text{wet}_i} \quad (4.14)$$

where  $n$  is the number of strips.

#### 4.2.3. Limitations of this method

Wing drag coefficient is determined by aerofoil (section) characteristics, based on strip theory. Strip theory assumes there is no spanwise interaction of the sections.

The flat plate analogy is valid for [26] (1) cases with aerofoil sections with a thickness-to-chord ratio of maximum 25%, (2) parts with smooth surface contours, and (3) small lift, or angle of incidence. The Flying-V analysis satisfies the first and the third item. The thickness-to-chord ratio varies per Flying V instance and depends on the inputs that are given, but for the cases treated in this thesis, the ratio of a *streamwise* aerofoil did not become higher than 0.17. With respect to the third item, flight condition is cruise, for which it is reasonable to assume a small angle of incidence. The second requirement for validity of the flat plate analogy, smooth surfaces, is not satisfied with this proposed Flying-V parametrisation because the Flying-V geometries have kinks.

The purpose of calculating the drag is to be used in the objective function of an aerodynamic optimisation. With that purpose in mind, a high fidelity drag estimation might not be needed and this empirical viscous drag estimation can be sufficient, as long as the *variations* of the objective function along the design space are a good reflection of the actual variations in the design landscape. When comparing the optimum Flying-V design to other designs, the actual magnitude of the drag is important, and a higher fidelity drag calculation can be required.

# 5

## Results

The parametrisation itself is a result of this research, based on the research objective. This chapter assesses the parametrisation. The robustness of the parametrisation is quantitatively evaluated by sampling the design space (section 5.1). Some cases are treated in more detail to qualitatively demonstrate the functionality of the parametrisation (section 5.2).

### 5.1. Robustness of the geometry parametrisation

Since the parametrisation should be able to be used in an aerodynamic optimisation, it is important that it is robust. Sóbester and Forrester define a parametric geometry's robustness as its "ability, in terms of design space proportion, to yield physically and geometrically sensible shapes" [14, p. 16]. Based on this definition, the robustness of the Flying-V parametrisation is evaluated. To do this the design space (subsection 5.1.1) is sampled (subsection 5.1.2).

The robustness is defined here as the fraction of feasible shapes that result from the total amount of samples (Equation 5.1).

$$\text{robustness} = \frac{N_{\text{feasible}}}{N} \quad (5.1)$$

#### 5.1.1. Design space

The negative null form of an optimisation problem is [28]:

$$\begin{aligned} &\text{minimise } f(\mathbf{x}) \\ &\text{subject to } \mathbf{h}(\mathbf{x}) = \mathbf{0} \\ &\quad \mathbf{g} \leq \mathbf{0} \\ &\quad \mathbf{x} \in \mathbb{X} \subseteq \mathbb{R}^n \end{aligned} \quad (5.2)$$

where  $n$  is the number of design variables,  $\mathbf{h} = \mathbf{0}$ ,  $\mathbf{g} \leq \mathbf{0}$  the system of *functional constraints*, and  $\mathbf{x} \in \mathbb{X}$  the *set constraint*. The subset  $\mathbb{X}$  is the design space. The subset that satisfies all constraints (the functional constraints and the set constraints) is the feasible domain.

#### 5.1.2. Sampling

The design space,  $\mathbb{X}$ , is sampled. The design space is only bounded by the *set* constraints (also known as the design variable bounds), and not by the *functional* constraints. Thus, the feasible domain is a subset of the design space  $\mathbb{X}$ . A sampling study is performed to estimate the robustness of the parametrisation. Based on the definition of robustness in section 5.1, it can be expressed as the feasible domain coverage of the design space. The bounds that define the design space of the Flying-V are listed in Appendix D.

The sampling strategy is LHS, using the LHS method of the Python pyDOE package. LHS is a popular design of experiments sampling method, intended for box-like domains. LHS subdivides the sampling domain (hypercube) into subdomains, which ensures a better design space coverage compared to simple random sampling.

For each sample, the feasibility of the shape is evaluated. The criteria to assess whether the shape is feasible are:

- For aerofoil sections 1, 2, and 3 (*InboardAerofoils*): the upper and lower rear aerofoil curve of section cannot intersect each other
- For aerofoil sections 1, 2, and 3 (*InboardAerofoils*): the rear aerofoil curves cannot intersect the oval fuselage section curve
- The position of the trailing edge point of section 4 cannot have a higher  $y$  location than the tip section

The feasibility percentage, or robustness, is then calculated using Equation 5.1. Figure 5.1 shows the results of different number of LHS samples. The feasibility percentage of the Flying-V parametrisation is around 29%, which can be seen in this figure. This indicates that the feasible domain covers approximately 29 % of the design space. A graphical overview of 100 samples is given in Appendix E, to serve as a visual impression of the design space.

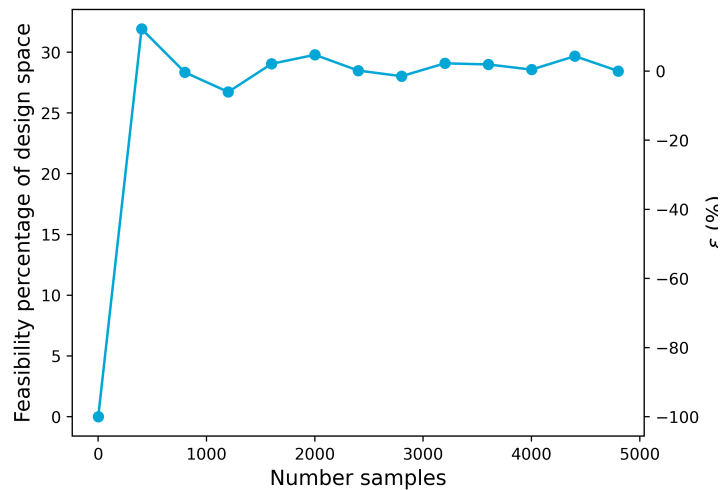


Figure 5.1: Convergence of LHS sample size

Most fuselage parameters are not design variables, and are therefore also not sampled. The fixed input parameters are listed in Table 5.1. The parametrisation has 50 design variable, if 12 Bernstein coefficients are used to parametrise the outboard aerofoils, which is the case for the cases treated in this thesis.

Table 5.1: Fixed input parameters for sampling study

Parameter	Symbol	Value	Unit
Untapered fuselage length (centre line length)	$L_1$	23.75	$m$
Tapered fuselage length (centre line length)	$L_3$	11.1	$m$
Leading edge distance between section 1 and 2	$l_2$	0	$m$
Width at input height of section 1	$w_{H_1}$	6.2	$m$
Width at input height of section 3	$w_{H_3}$	5.8	$m$
Wing span	$b$	60.4	$m$
Cabin height of oval section 1	$H_{2_1}$	2.25	$m$
Cabin height of oval section 3	$H_{2_3}$	1.75	$m$
Height of input width of section 1	$H_{w_1}$	0.6	$m$
Height of input width of section 3	$H_{w_3}$	0.6	$m$

## 5.2. Case studies

The capability of the parametrisation and aerodynamic analysis module is demonstrated in more detail by evaluating four cases. The input values for each of these cases can be found in [Appendix B](#). The first case is a Flying-V geometry that aims to approximate the Flying-V OML design of Faggiano [5] with the new parametrisation ([subsection 5.2.1](#)). The second ([subsection 5.2.2](#)), third ([subsection 5.2.3](#)), and fourth ([subsection 5.2.4](#)) case are Flying-V family members that satisfy the updated cabin requirements that result from the cabin design. The Flying-V family members are created by varying the length of the constant cross-section wing- and cabin trunk ([Figure 5.2](#)).

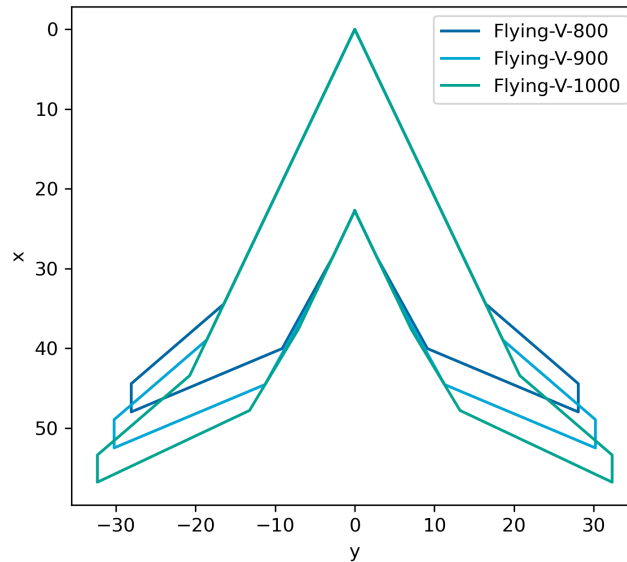


Figure 5.2: Wing planform shapes of the (not yet optimised) Flying-V family

In the following subsections, these cases will be referred to with numbers. The Flying-V design by Faggiano is also referred to with a number. The resulting list of configurations is:

0. Faggiano's Flying-V design
1. An approximation of Faggiano's design using the proposed parametrisation
2. A Flying-V-800
3. A Flying-V-900
4. A Flying-V-1000

The geometrical properties of each of these cases are summarised in [Table 5.2](#) and the aerodynamic results are summarised in [Table 5.3](#). The rest of this section contains more elaborate descriptions of the cases and the results.

Table 5.2: Geometrical properties of the current Flying-V design

Case	$A_{\text{floor}} (m^2)$	$S_{\text{wing}} (m^2)$	$\bar{c} (m)$	$S_{\text{wet}} (m^2 \text{ e}3)$	$V_{\text{fuselage}} (\times 10^3 m^3)$	$V_{\text{OML}} (\times 10^3 m^3)$	$\frac{V_{\text{fuselage}}}{V_{\text{OML}}} (\%)$
0	321	883	17.9	1.92	1.00	1.67	59.9
1	332	882	17.9	1.91	1.06	1.54	68.8
2	368	762	17.4	1.67	1.19	1.45	82.1
3	430	860	18.0	1.89	1.39	1.71	81.3
4	491	927	18.2	2.05	1.52	1.74	87.4

Table 5.3: Aerodynamic coefficients of the different cases

Parameter	$C_L$	$C_D$ (counts)	$C_{D_{\text{visc}}}$ (counts)	$C_{D_{\text{inv}}}$ (counts)	$\frac{C_L}{C_D}$
0: Faggiano's Flying-V (re-analysed)	0.266	99.4	48.3	51.1	26.7
1: Approximate Faggiano's shape	0.264	114	47.7	66.2	23.2
2: Flying-V-800	0.265	166	49.3	117	16.0
3: Flying-V-900	0.265	154	48.8	105	17.2
4: Flying-V-1000	0.265	146	48.4	97.8	18.1

### 5.2.1. Case 1 - an approximation of Faggiano's design

The input values of this configuration are manually selected to approximate Faggiano's Flying-V planform shape and reference area. In this subsection, this case's geometry and that of Faggiano are compared, as well as their aerodynamic results. This should give some indication about the effect of the parametrisation on the geometry, and therefore on the aerodynamics.

Some input parameters, such as the sweep, the span, and the Bernstein coefficients of the tip section have remained unchanged with respect to Faggiano's parametrisation. The values of these variables for this case are therefore the same as the single step optimised shape of Faggiano [5]. The fuselage dimensions and planform chord  $c_1'$  could be computed relatively easy from Faggiano's optimum design vector. Other parameters could not be derived easily. These are the rear wing parameters, and the Bernstein coefficients of section 4. These are the parameters that specify the profile shape of wing sections 1, 2, 3, and 4.

#### Geometry

The parametrisation strategy proposed in this thesis affects the planform shape (Figure 5.3). The leading edges of the two planforms coincide, which is easily achieved because both parametrisations have the leading edge sweep of the inboard wing and the outboard wing as inputs. All the wing trunks in Faggiano's geometry parametrisation are tapered, whereas that of the proposed parametrisation features a combination of a constant cross-section wing trunk, three tapered wing trunks, and a connection trunk. Consequently, the trailing edges are different. Another difference that can be observed from Figure 5.3 is the orientation of the wing loft profiles.

Because almost all wing trunks are linear lofts, and the wing is composed of multiple wing trunks, the OML is not a smooth surface: at the border between two wing trunks, the surface is G0 continuous. This is also the case in the former parametrisation, except that these discontinuities in smoothness are oriented differently. The inboard profiles (section 1, 2, and 3) of the proposed parametrisation are positioned perpendicular to the centreline of the fuselage. Section 4's orientation depends directly on the input parameter  $\delta$ , so this section is not per definition parallel to the free-stream. It is possible to position section 4 to be parallel to the freestream, (corresponding to  $\delta = 0$ ), but this causes the chord length to increase (all other inputs remaining the same). Because the old parametrisation has its loft profiles oriented in streamwise planes, and these profiles have at least G1 continuity, a streamwise cut also has G1 continuity. These profiles are also at least G1 continuous. However, the streamwise cuts of the new parametrisation that cross the loft profiles are only G0 continuous (Figure 5.4). This is particularly well visible in streamwise cuts that cross section 4.

This configuration has a higher fuselage volume than Faggiano's Flying-V, which is mainly due to the addition of the connection trunk. The fuselage volume to OML volume ratio of this geometry is 10% higher than that of Faggiano's design. The new parametrisation does not have excess space between the tapered fuselage trunk and the OML any more, which contributes to this more efficient use of volume. The A350-900 has a maximum fuel capacity of 141 m<sup>3</sup>. If the Flying-V is indeed 25% more fuel efficient in cruise conditions, the new Flying-V-900 design should at least be capable of carrying 106 m<sup>3</sup> of fuel. The difference between the OML volume and fuselage volume is 484 m<sup>3</sup>, so in theory there should be sufficient volume still available to carry the fuel.

#### Aerodynamic results

Near the root of the OML, the pressure contours of configuration 1 (Figure 5.5) look similar to that of Faggiano's design (Figure 5.6). Around approximately 30-50% of the semi-span, the pressure contours indicate strong adverse pressure gradients on the upper surface. The outboard wing geometry is fairly

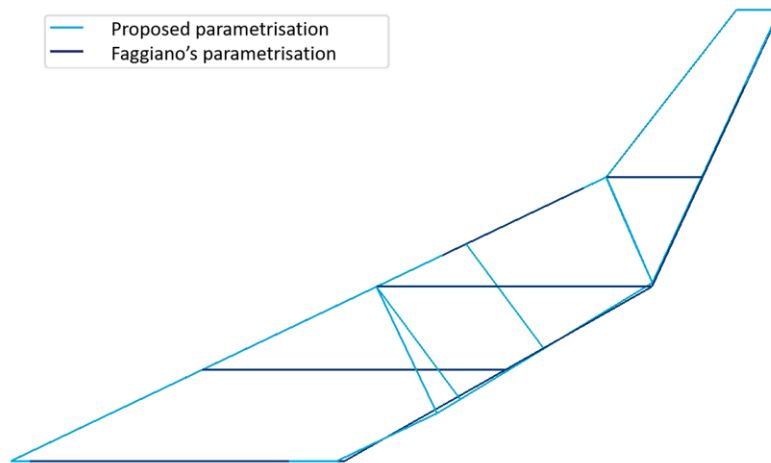


Figure 5.3: Comparison of Flying-V planform shapes between the Faggiano parametrisation and the proposed parametrisation

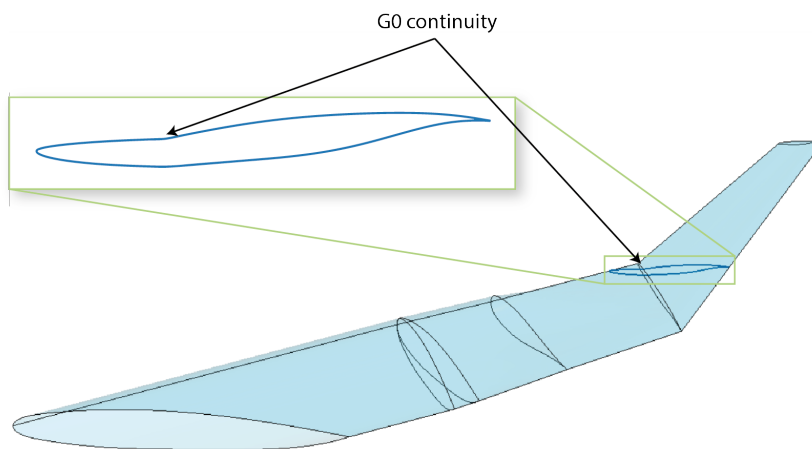


Figure 5.4: Semi wing geometry of case 1, with a streamwise cut at  $0.6 \frac{b}{2}$

similar to that of the current Flying V, which is also reflected in the pressure contours. Note that by assuming inviscid flow, possible separation is not captured by the flow solution. The lift-to-drag ratio of this configuration is 23.2, which is lower than that of Faggiano's Flying-V design. The viscous drag approximation also does not account for pressure drag due to flow separation, thus the effect of flow separation is not included in the lift-to-drag ratio.

### 5.2.2. Case 2 - a Flying-V-800

A cabin layout for the Flying-V-800 that includes the positions and size of the passenger seats, cargo containers, galleys, lavatories, and doors is shown in [Figure 5.7](#). The Flying-V-800 is the smallest of the Flying-V family.

#### Flying-V-800 geometry

The Flying-V-800 has a span of 56.1 m, whereas Faggiano's design has a span of 65.0 m. The length of the constant cross-section fuselage trunk,  $L_1$ , is 18.75 m. Between the family members, the total fuselage size is varied by varying this particular length. In this aircraft, the distance between section 3 and 4 is smaller than for the previous case, and the result of that is clearly visible in a streamwise cut ([Figure 5.8](#)). Section 3 is the most outboard positioned section that is an instance of the class `InboardAerofoil`, thus it marks the end of the fuselage. The oval needs to have a certain thickness to accommodate the cargo containers, while section 4 is not restricted by the fuselage thickness dimensions. Positioning these profiles close to each other causes the discontinuities in smoothness to be more sharp.

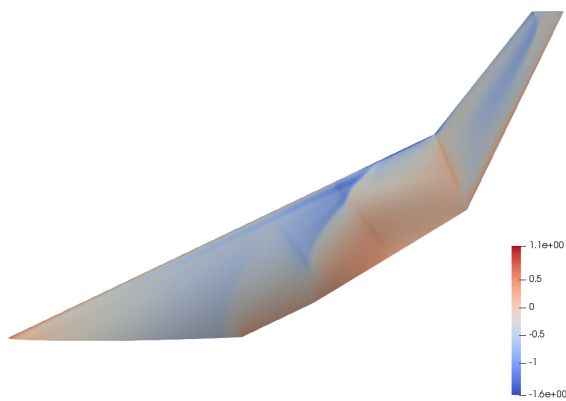
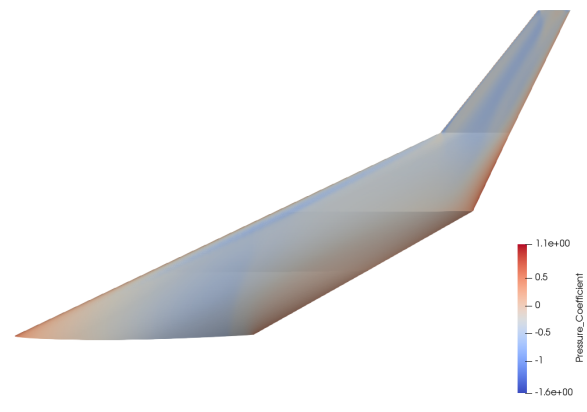
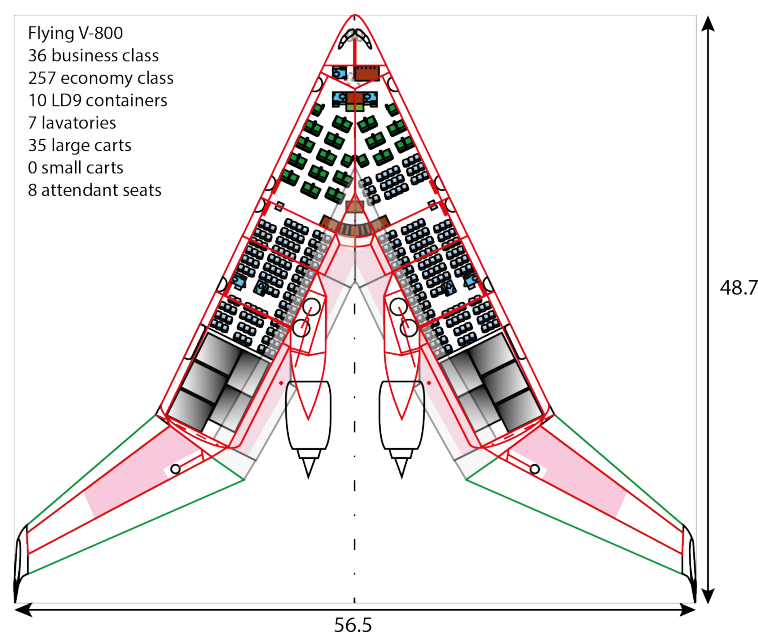
Figure 5.5: Case 1  $C_p$ ,  $Ma = 0.85$ ,  $C_L = 0.266$ Figure 5.6: Former Flying-V OML  $C_p$  contours,  $Ma = 0.85$ ,  $C_L = 0.266$ 

Figure 5.7: Flying-V-800 planform, courtesy of R. Vos

### Flying-V-800 aerodynamic results

The pressure contours of this aircraft in cruise conditions show similar behaviour to that of case 1, which are high adverse pressure gradients on tapered wing trunk (Figure 5.9). Around the transition from inboard to outboard wing, a region of low pressure is encountered and after the decrease in thickness a region of lower pressure is encountered. This can be related to the aerofoil shape illustrated in Figure 5.8, where near the trailing edge of the streamwise cut, the curvature of the aerofoil curve is first concave and subsequently convex.

### 5.2.3. Case 3 - a Flying-V-900

The third case is the middle sized family member. It has a span of 60.4 m, and  $L_1$  is 23.75 m (5 m longer than that of the Flying-V-800). In terms of intended payload capacity, this is the family member that Faggiano's design is equivalent to. After the aerodynamic design in 2016, a planform layout of the cabin was created (Figure 5.10). Based on this, it became evident that the containers and the passengers do not actually fit inside the fuselage. The new fuselage size requirements have been implemented into this case study. The leading edge kink location and the span are kept the same as

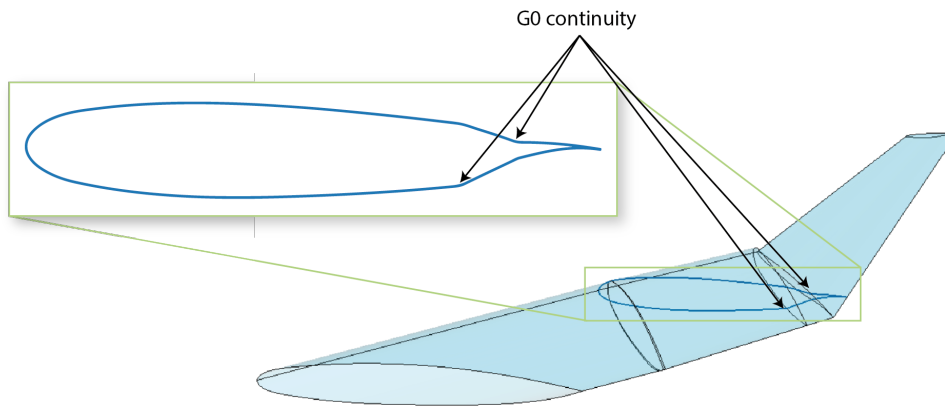


Figure 5.8: Semi wing geometry of case 2, with a streamwise cut at  $0.4 \frac{b}{2}$

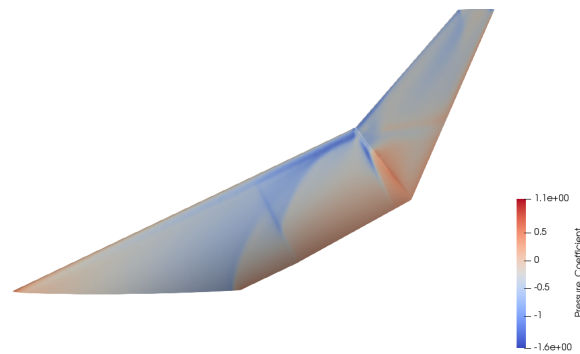


Figure 5.9: Flying-V-800  $C_p$  contours,  $Ma = 0.85$ ,  $C_L = 0.27$

for case 1 and the Faggiano Flying-V design.

#### Flying-V-900 geometry

The fuselage is approximately 6 m longer than that of Faggiano's design and the fuselage volume is  $300 \text{ m}^3$  higher than that of case 1. The transition from inboard to outboard wing is the same as for the previous case.

#### Flying-V-900 aerodynamic results

For this Flying V configuration, the pressure coefficient contours also show that the kinks in the OML affect the flow. The untapered fuselage is longer and therefore a large inboard area is created without discontinuities in the curvature, which reflects in smooth pressure contours (Figure 5.11). The transition to the tapered inboard wing shows the same behaviour as for the previous case. At the transition between the inboard and outboard wing, where the thickness of the wing rapidly decreases, the Mach contours show a strong decrease in Mach number (Figure 5.12).

The lift-to-drag ratio of this configuration is 17.2, which is still substantially lower than that of case 1, but it is higher than that of the Flying-V-800 (Table 5.3).

#### 5.2.4. Case 4 - a Flying-V-1000

The largest of the Flying-V family is the Flying-V-1000 (Figure 5.13). It has the same span as the A350-900 and Faggiano's design. So it actually fits more payload within the same span.

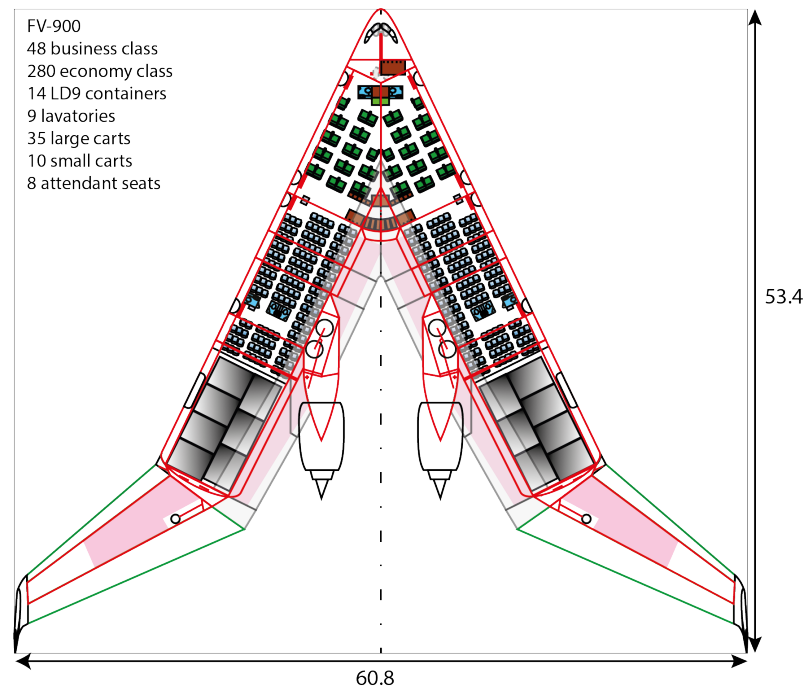


Figure 5.10: Flying-V-900 planform, courtesy of R. Vos

#### Flying-V-1000 geometry

The fuselage of the Flying-V-1000 is 5 m longer than that of the Flying-V-900, and approximately 11 m longer than Faggiano's cabin. Because case 2, 3, and 4 all have a similar geometry at the transition from inboard to outboard wing, an example is shown here to illustrate that the shape is considerably improved if a thicker aerofoil is used for section 4. If the aerofoil of section 4 is replaced by a NACA0020 aerofoil, which is a relatively thick aerofoil, the thickness decrease around the kink is already less sharp (Figure 5.14). There is still a "dent" in the aerofoil curve, but this is already an improvement with respect to the thinner aerofoil. The Bernstein coefficient parametrisation is already more flexible than the NACA 4 digit aerofoil and an aerodynamic optimisation may be able to find the right combination of coefficients to smooth this transition.

#### Flying-V-aerodynamic results

The pressure contours are shaped similar to that of the Flying-V-800 and Flying-V-900, except that this aircraft has an even larger constant-cross-section region. Therefore the region with smooth pressure contours is also larger (Figure 5.15). Compared to the pressure contours of the Flying-V-900 and -1000, the gradients are also less sharp.

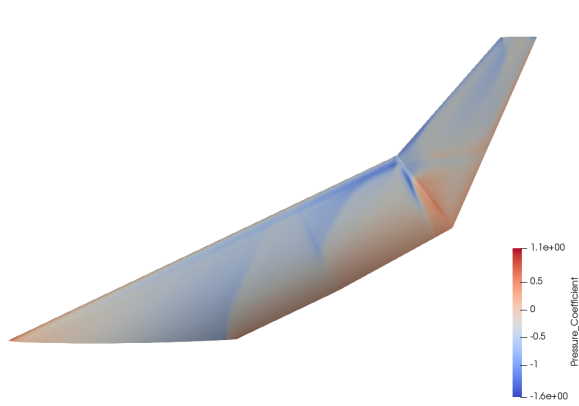


Figure 5.11: Flying-V-900  $c_p$  contours,  $Ma = 0.85$ ,  $C_L = 0.266$

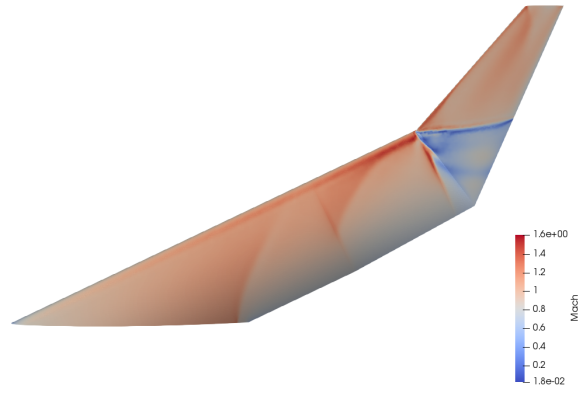


Figure 5.12: Flying-V-900 Mach contours,  $Ma = 0.85$ ,  $C_L = 0.266$

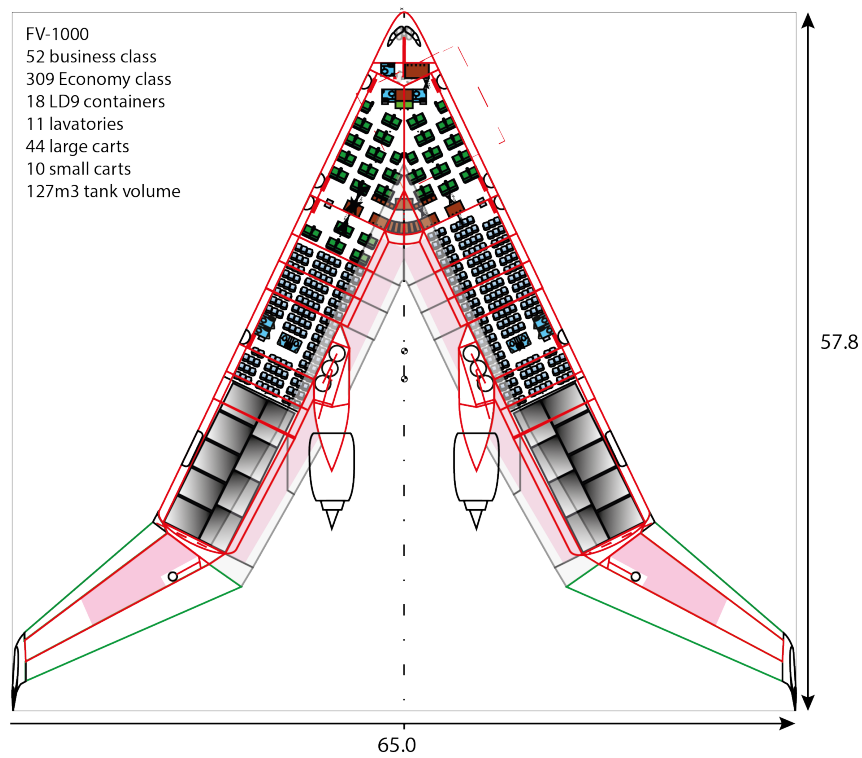


Figure 5.13: Flying-V-1000 planform, courtesy of R. Vos

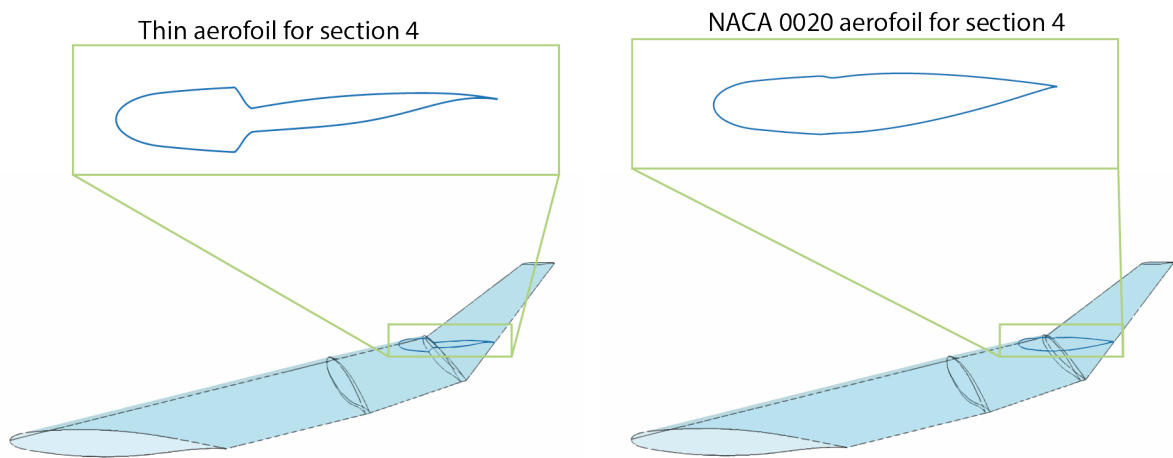


Figure 5.14: Flying-V-1000 with two different section 4 shapes

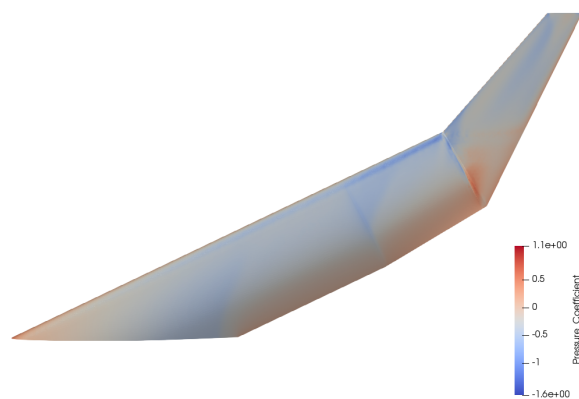


Figure 5.15: Flying-V-1000  $C_p$  contours,  $Ma = 0.85$ ,  $C_L = 0.266$

# 6

## Conclusions and recommendations

The research objective of the work presented in this thesis is to create a new parametrisation of the Flying-V Outer Mould Line that includes cabin design flexibility and manufacturability, and that can be used in an aerodynamic optimisation routine. To do this, a geometry parametrisation is created of the Flying-V fuselage and the wing that is built around it. This parametrisation is implemented in an engineering application, built using the python language in combination with ParaPy. This Flying-V design application can generate a three-dimensional Flying-V shape, which can be meshed and fed to an aerodynamic analysis module that activates the Euler analysis of Stanford University Unstructured and an empirical viscous drag estimation.

The results of the research is an evaluation of the parametrisation that is created. One part of this evaluation is the determination of the robustness of the geometry parametrisation. The other part is a qualitative demonstration of the shapes and aerodynamic results of a number of cases.

Based on the results of the robustness study and the case studies, the conclusions of this research are drawn ([section 6.1](#)). Finally, recommendations for future work are given ([section 6.2](#))

### 6.1. Conclusions

The Flying-V outer mould line parametrisation proposed in this thesis includes cabin design flexibility, by allowing the dimensions of the two fuselage trunks to be specified as input parameters. The outer mould line shape depends on the fuselage shape. The parametrisation includes manufacturability by implementing a constant cross-section wing and cabin trunk, by primarily using linear lofted shells, by orienting the wing loft profiles in the same planes as the wing ribs, and by letting the skin of the fuselage double as skin for the leading edge of the wing.

The main geometrical difference between the former and the proposed parametrisation is the orientation of the surface smoothness discontinuities. All surface kinks of the old parametrisation were oriented streamwise, whereas in the new parametrisation the inboard kinks are oriented perpendicular to the cabin centre line and the orientation of the profile between the inboard and outboard wing is directly adjustable by an input parameter.

Flying-V shapes resulting from updated cabin dimension requirements dimensions show that if the outboard wing shape is kept the same, the increased cabin size results in a rapid thickness decrease between the outboard oval profile and the aerofoil between the inboard and outboard wing. This rapid thickness decrease in combination with the strategy to use multiple linear lofts results in streamwise shapes with high curvatures and curvature discontinuities.

Euler analyses of four Flying-V geometries reveal that at the leading edge of the inboard tapered wing trunks experience high suction peaks and high adverse pressure gradients. These analyses also reveal that the proposed parametrisation can create sharp edges in the outer mould line if two profiles close to each other have different thicknesses. Aerodynamically speaking, this is unfavourable.

An approximation of the former Flying-V shape is created and analysed, using the parametrisation proposed in this research. Compared to a re-analysis of the outer mould line shape of the former Flying-V design, the shape created with the new parametrisation has a 13% lower lift-to-drag ratio. The lift-to-drag ratio is estimated based on a drag coefficient that is the sum of an Euler analysis drag

coefficient and a semi-empirical viscous drag coefficient. The lift-to-drag ratio of the Flying-V-1000, the largest of the Flying-V family that has the same span as the former Flying-V design and, is estimated to be 32% lower than the lift-to-drag coefficient of the former Flying-V design. Note that the new configuration geometries that are analysed in this study are no optima and as such, their comparison with the former (optimal) design is not valid. Nonetheless, the findings indicate that the enlarged cabin negatively affects the lift-to-drag ratio.

The robustness of the parametrisation is expressed in terms of feasible domain coverage of the design space. This is estimated by sampling the design space and evaluating the sample's feasibility, using the Latin Hypercube Sampling method. The criteria for feasibility are that the inboard aerofoil curves may not cross each other, may not cross the fuselage, and that the position of the wing profile cannot be more outboard than the tip profile. The resulting robustness is 29%, which indicates that the method of parametrising the inboard aerofoils, and the orientation of the outboard wing profile, is not very efficient.

## 6.2. Recommendations

This research is the first step towards a Flying-V design that includes manufacturability, and design flexibility. The next step is to use this parametrisation in an aerodynamic optimisation routine to actually obtain an optimum, which will be the next version of the Flying-V design. This optimum can then be compared to the former aerodynamic design in order to draw conclusions about the effect of cabin design flexibility and manufacturability on the aerodynamic performance of the Flying-V. The constraints that are proposed to be included in the optimisation are:

- Rear aerofoil curves should not intersect each other intersecting
- Rear aerofoil curves should not intersect the oval curve
- The  $y$  position of the outboard wing sections should not be larger than the semispan

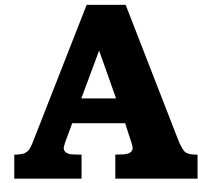
The parametrisation itself can be improved in a number of ways:

- The robustness study showed that the parametrisation is prone to generate shapes that intersect themselves. These intersections happen at the rear wing curves. Because these are polynomials, the curves can easily shoot into a direction and create a curve that does not resemble an aerofoil any more. It is recommended to investigate possibilities to use a different parametrisation for the rear wing curves.
- The criteria that were used to assess the feasibility of the shape are equivalent to the constraints that have to be used in an optimisation. It is recommended that instead of assessing whether the aerofoil thickness is greater than zero (i.e. assessing whether an aerofoil curve intersects itself), a minimum thickness greater than zero can be implemented in this constraint. This will improve the design from a manufacturability standpoint.
- This parametrisation intentionally leads to an outer mould line that is not continuously smooth. There are regions that have G1 continuity and even G0 continuity. The idea behind this parametrisation is to minimise the complexity of the curvatures. To improve the smoothness of the aircraft's outer surface to G2 continuity would increase the amount of double curvature in the design. The drawback is that it sacrifices manufacturability of the design.

# Bibliography

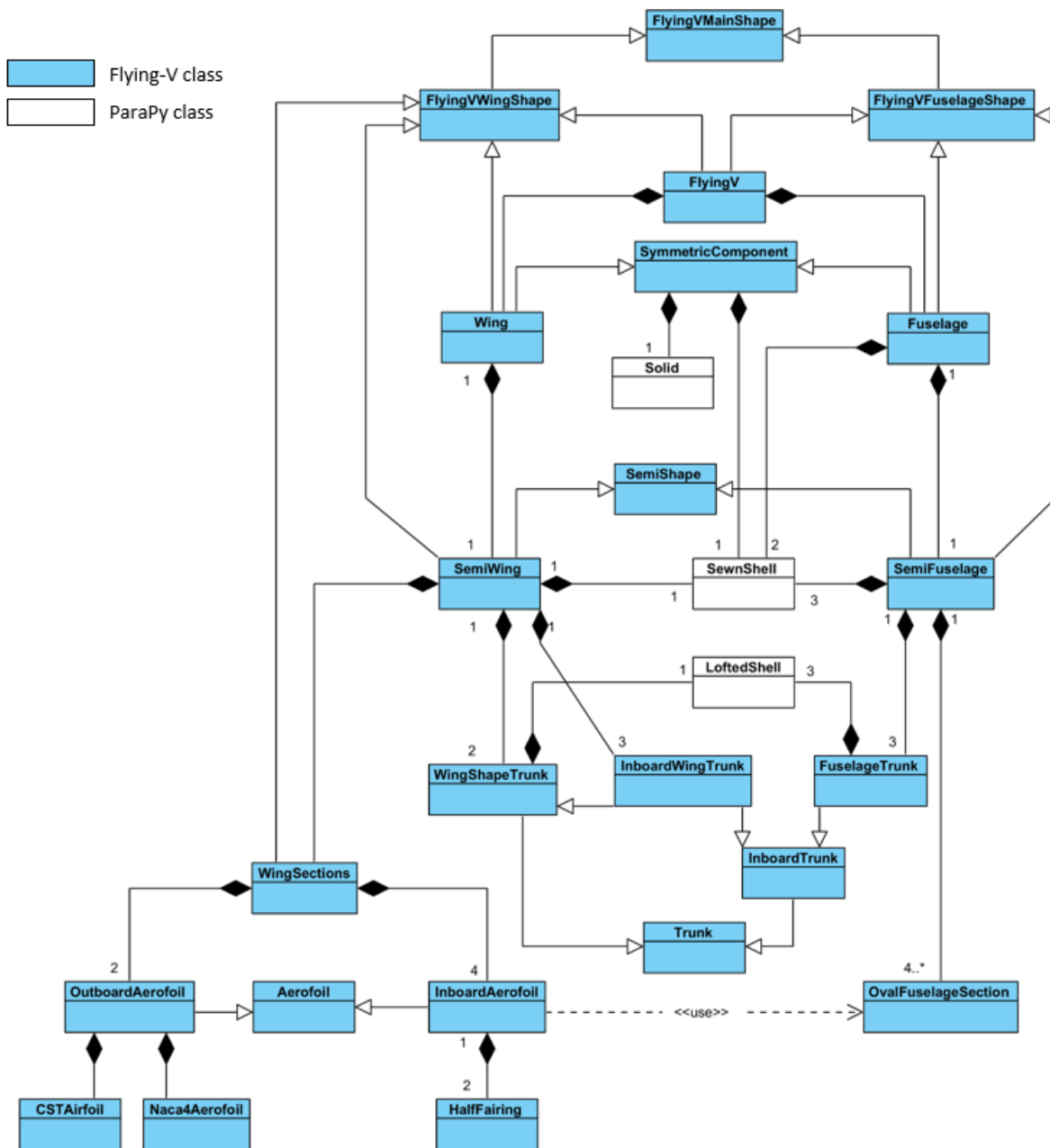
- [1] L. van der Schaft, *Development, Model Generation and Analysis of a Flying V Structure Concept*, [Master's thesis](#), Delft University of Technology (2017).
- [2] S. R. Shankar and D. G. Jansson, *A generalized methodology for evaluating manufacturability*, in [Concurrent Engineering](#) (Springer US, Boston, MA, 1993) pp. 248–263.
- [3] N. Qin, A. Vavalle, A. Le Moigne, M. Laban, K. Hackett, and P. Weinerfelt, *Aerodynamic considerations of blended wing body aircraft*, [Progress in Aerospace Sciences](#) **40**, 321 (2004).
- [4] J. Benad, *The Flying V - A New Aircraft Configuration for Commercial Passenger Transport*, (Deutsche Gesellschaft für Luft- und Raumfahrt - Lilienthal-Oberth e.V., 2015).
- [5] F. Faggiano, *Aerodynamic Design Optimization of a Flying V Aircraft*, [Master's thesis](#), Delft University of Technology (2016).
- [6] M. Claeys, *Flying V and Reference Aircraft Structural Analysis and Mass Comparison*, [Master's thesis](#), Delft University of Technology (2018).
- [7] B. Rubio Pascual, *Engine-Airframe Integration for the Flying-V*, [Master's thesis](#), Delft University of Technology (2018).
- [8] R. Viet, *Analysis of the flight characteristics of a highly swept cranked flying wing by means of an experimental test*, [Master's thesis](#), Delft University of Technology (2019).
- [9] M. Palermo, *The Longitudinal Static Stability and Control Characteristics of a Flying V Scaled Model: An Experimental and Numerical Investigation*, [Master's thesis](#), Delft University of Technology (2019).
- [10] M. Hoogreef, *The Oval Fuselage: A New Structural Design Concept for Blended Wing Body Cabins*, (2012).
- [11] D. P. Raymer, *Aircraft Design: A Conceptual Approach*, 5th ed. (American Institute of Aeronautics and Astronautic, Inc, 2012).
- [12] P. Selvaraj, P. Radhakrishnan, and M. Adithan, *An integrated approach to design for manufacturing and assembly based on reduction of product development time and cost*, [The International Journal of Advanced Manufacturing Technology](#) **42**, 13 (2009).
- [13] G. Boothroyd, *Product design for manufacture and assembly*, [Computer-Aided Design](#) **26**, 505 (1994).
- [14] A. Sóbester and A. I. J. Forrester, *Aircraft Aerodynamic Design: Geometry and Optimization*, 1st ed., edited by P. Belobaba, J. Cooper, and A. Seabridge (John Wiley & Sons, Ltd, 2015).
- [15] D. Costin and B. Wang, *Optimum Design of a Composite Structure with Manufacturing Constraints*, [Thin-Walled Structures](#) **17**, 185 (1993).
- [16] T. van der Laan and L. Hootsmans, *Consequences of Multi or Single disciplinary optimization results on aircraft component cost and weight*, in [2018 Aviation Technology, Integration, and Operations Conference](#) (American Institute of Aeronautics and Astronautics, 2018).
- [17] S. K. Gupta, W. C. Regli, D. Das, and D. S. Nau, *Automated manufacturability analysis: A survey*, [Research in Engineering Design](#) **9**, 168 (1997).

- [18] M. Rais-Rohani and Z. Huo, *Analysis and optimization of primary aircraft structures based on strength, manufacturability, and cost requirements*, in *40th Structures, Structural Dynamics, and Materials Conference and Exhibit* (American Institute of Aeronautics and Astronautics, Reston, Virginia, 1999).
- [19] R. Vos, F. Geuskens, and M. Hoogreef, *A New Structural Design Concept for Blended Wing Body Cabins*, in *53rd AIAA/ASME/ASCE/AHS/ASC Structures, Structural Dynamics and Materials Conference* (American Institute of Aeronautics and Astronautics, 2012).
- [20] R. K. Schmidt, *Masters Thesis: A Semi-Analytical Weight Estimation Method for Oval Fuselages in Novel Aircraft Configurations*, *Master's thesis*, Delft University of Technology (2013).
- [21] B. M. Kulfan, *Universal Parametric Geometry Representation Method*, *Journal of Aircraft* **45**, 142 (2008).
- [22] K. E. Atkinson, *An Introduction to Numerical Analysis*, 2nd ed. (John Wiley & Sons, Inc, 1989).
- [23] T. Vogeltanz, *Application for calculation of mean aerodynamic chord of arbitrary wing planform*, in *AIP Conference Proceedings*, Vol. 1738, p. 120018.
- [24] R. M. Cummings, W. H. Mason, S. A. Morton, and D. R. McDaniel, *Applied computational aerodynamics: a modern engineering approach* (Cambridge University Press, 2015).
- [25] F. Palacios, M. R. Colonno, A. C. Aranake, A. Campos, S. R. Copeland, T. D. Economon, A. K. Lonkar, T. W. Lukaczyk, T. W. R. Taylor, and J. J. Alonso, *Stanford University Unstructured (SU2): An open-source integrated computational environment for multi-physics simulation and design*, in *51st AIAA Aerospace Sciences Meeting including the New Horizons Forum and Aerospace Exposition* (American Institute of Aeronautics and Astronautics, 2013).
- [26] E. Torenbeek, *Synthesis of Subsonic Airplane Design* (1982).
- [27] J. H. Ferziger, M. Perić, and R. L. Street, *Computational Methods for Fluid Dynamics*, 4th ed. (2020).
- [28] P. Y. Papalambros and D. J. Wilde, *Principles of Optimal Design: Modeling and Computation*, 2nd ed. (Cambridge University Press, 2000).



# Class diagram

-  Flying-V class
-  ParaPy class





# B

## Input files

Table B.1: Input parameters of case 1: an approximation of Faggiano's geometry

Parameter	Symbol	Value	Unit
<b>Fuselage planform</b>			
Untapered fuselage length (centre line length)	$L_1$	21.53	m
Tapered fuselage length (centre line length)	$L_3$	7.00	m
Leading edge distance between section 1 and 2	$l_2$	0	m
Width at input height of section 1	$w_{H_1}$	5.97	m
Width at input height of section 3	$w_{H_3}$	3.3	m
<b>Cargo containers (only for visualisation)</b>			
Spanwise spacing between containers	$y_{cargo}$	0.01	m
Chordwise spacing between containers	$x_{cargo}$	0.01	m
Type of container(s)		'LD-4'	-
Leading row positioning of containers		True	-
Number of containers	$n_{containers}$	14	-
<b>Wing planform</b>			
Wing span	$b$	65.0	m
Planform chord of section 1 fraction	$\bar{c}'_1$	1.25	-
Inboard wing leading edge sweep angle	$\Lambda_{in}$	64.5	°
Outboard wing leading edge sweep angle	$\Lambda_{out}$	37.9	°
Dihedral of wing trunk 4	$\Gamma_4$	-0.1785	°
Dihedral of wing trunk 5	$\Gamma_5$	5.825	°
Incidence of aerofoil 4	$i_4$	0.4	°
Incidence of tip aerofoil	$i_5$	-4.37	°
Taper ratio	$\lambda$	0.133	-
Length 4 fraction	$\bar{L}_4$	0.285	-
Planform chord of section 3 fraction	$\bar{c}'_3$	1.84	-
Angle between aircraft's x axis and aerofoil 4's x axis	$\delta$	66.50	°
<b>Oval</b>			
Cabin height of oval section 1	$H_{2_1}$	2.25	m
Cabin height of oval section 3	$H_{2_3}$	1.75	m
Height of input width of section 1	$H_{w_1}$	0.6	m
Height of input width of section 3	$H_{w_3}$	0.6	m
Crown height of oval section 1	$H_{1_1}$	0.6	m
Crown height of oval section 3	$H_{1_3}$	0.2	m
Keel height of oval section 1	$H_{3_1}$	0.7	m
Keel height of oval section 3	$H_{3_3}$	0.2	m
<b>Rear aerofoil</b>			
Upper rear wing polynomial coefficient of section 1	$c_{up_1}$	1e-5	$m^{-3}$
Upper rear wing polynomial coefficient of section 3	$c_{up_3}$	-1e-4	$m^{-3}$
Lower rear wing polynomial coefficient of section 1	$c_{low_1}$	0.002	$m^{-3}$
Lower rear wing polynomial coefficient of section 3	$c_{low_3}$	0.0001	$m^{-3}$
Vertical position of trailing edge in section 1	$Z_{TE_1}$	-0.3	m
Vertical position of trailing edge in section 3	$Z_{TE_3}$	-0.04	m
Start position of upper rear wing curve 1	$\bar{x}_{sup_1}$	0.4	-
Start position of upper rear wing curve 3	$\bar{x}_{s_{low_3}}$	0.3	-
Start position of lower rear wing curve 1	$\bar{x}_{sup_1}$	0.4	-
Start position of lower rear wing curve 3	$\bar{x}_{s_{low_3}}$	0.3	-
Upper Bernstein coefficients of section 4	$A_{u_4}$	[0.088, 0.066, 0.21, 0.079, 0.24, 0.23]	
Lower Bernstein coefficients of section 4	$A_{l_4}$	[-0.13, -0.084, -0.031, -0.31, 0.069, 0.10]	
Upper Bernstein coefficients of tip section (5)	$A_{u_{tip}}$	[0.14, 0.068, 0.20, 0.078, 0.14, 0.29]	
Lower Bernstein coefficients of tip section (5)	$A_{l_{tip}}$	[-0.099, -0.084, -0.025, -0.39, 0.061, 0.17]	
<b>Flight mechanics</b>			
Cruise weight	$w_{cruise}$	2e5	kgf
Cruise Mach number	$Ma_{cruise}$	0.85	-
<b>Other settings</b>			
Position section by floor		True	-
Number of profiles for torus trunk	$n_{loft_2}$	10	-
Distance from global origin to wing loft origin	$X_0$	10	m

Table B.2: Input parameters of case 2: a Flying-V-800

Parameter	Symbol	Value	Unit
<b>Fuselage planform</b>			
Untapered fuselage length (centre line length)	$L_1$	18.75	m
Tapered fuselage length (centre line length)	$L_3$	11.1	m
Leading edge distance between section 1 and 2	$l_2$	0	m
Width at input height of section 1	$w_{H_1}$	6.2	m
Width at input height of section 3	$w_{H_3}$	5.8	m
<b>Cargo containers (only for visualisation)</b>			
Spanwise spacing between containers	$y_{\text{cargo}}$	0.01	m
Chordwise spacing between containers	$x_{\text{cargo}}$	0.01	m
Type of container(s)		'LD-9'	-
Leading row positioning of containers		[True, True, True]	-
Trailing row positioning of containers		[False, False]	-
Number of containers	$n_{\text{containers}}$	None	-
<b>Wing planform</b>			
Wing span	$b$	56.1	m
Planform chord of section 1 fraction	$\bar{c}'_1$	1.16	-
Inboard wing leading edge sweep angle	$\Lambda_{\text{in}}$	64.5	°
Outboard wing leading edge sweep angle	$\Lambda_{\text{out}}$	40.7	°
Dihedral of wing trunk 4	$\Gamma_4$	-0.1785	°
Dihedral of wing trunk 5	$\Gamma_5$	5.825	°
Incidence of aerofoil 4	$i_4$	0.4	°
Incidence of tip aerofoil	$i_5$	-4.37	°
Taper ratio	$\lambda$	0.156	-
Length 4 fraction	$\bar{L}_4$	0.0110	-
Planform chord of section 3 fraction	$\bar{c}'_3$	1.21	-
Angle between aircraft's x axis and aerofoil 4's x axis	$\delta$	52.6	°
<b>Oval</b>			
Cabin height of oval section 1	$H_{2,1}$	2.25	m
Cabin height of oval section 3	$H_{2,3}$	1.75	m
Height of input width of section 1	$H_{w1}$	0.6	m
Height of input width of section 3	$H_{w3}$	0.6	m
Crown height of oval section 1	$H_{1,1}$	0.6	m
Crown height of oval section 3	$H_{1,3}$	0.2	m
Keel height of oval section 1	$H_{3,1}$	0.7	m
Keel height of oval section 3	$H_{3,3}$	0.2	m
<b>Rear aerofoil</b>			
Upper rear wing polynomial coefficient of section 1	$c_{\text{up}1}$	1e-5	$\text{m}^{-3}$
Upper rear wing polynomial coefficient of section 3	$c_{\text{up}3}$	1e-5	$\text{m}^{-3}$
Lower rear wing polynomial coefficient of section 1	$c_{\text{low}1}$	0.002	$\text{m}^{-3}$
Lower rear wing polynomial coefficient of section 3	$c_{\text{low}3}$	0.0001	$\text{m}^{-3}$
Vertical position of trailing edge in section 1	$z_{\text{TE}1}$	-0.3	m
Vertical position of trailing edge in section 3	$z_{\text{TE}3}$	-0.04	m
Start position of upper rear wing curve 1	$\tilde{x}_{\text{sUP}1}$	0.4	-
Start position of upper rear wing curve 3	$\tilde{x}_{\text{sUP}3}$	0.3	-
Start position of lower rear wing curve 1	$\tilde{x}_{\text{sUP}1}$	0.4	-
Start position of lower rear wing curve 3	$\tilde{x}_{\text{sUP}3}$	0.3	-
Upper Bernstein coefficients of section 4	$A_{u4}$	[0.088, 0.066, 0.21, 0.079, 0.24, 0.23]	
Lower Bernstein coefficients of section 4	$A_{l4}$	[-0.13, -0.084, -0.031, -0.31, 0.069, 0.20]	
Upper Bernstein coefficients of tip section (5)	$A_{u\text{tip}}$	[0.14, 0.068, 0.20, 0.078, 0.14, 0.29]	
Lower Bernstein coefficients of tip section (5)	$A_{l\text{tip}}$	[-0.099, -0.084, -0.025, -0.39, 0.061, 0.17]	
<b>Flight mechanics</b>			
Cruise weight	$w_{\text{cruise}}$	2e5	kgf
Cruise Mach number	$Ma_{\text{cruise}}$	0.85	-
<b>Other settings</b>			
Position section by floor		False	-
Number of profiles for torus trunk	$n_{\text{loft}2}$	10	-
Distance from global origin to wing loft origin	$X_0$	10	m

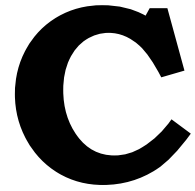
Table B.3: Input parameters of case 2: a Flying-V-900

Parameter	Symbol	Value	Unit
<b>Fuselage planform</b>			
Untapered fuselage length (centre line length)	$L_1$	23.75	m
Tapered fuselage length (centre line length)	$L_3$	11.1	m
Leading edge distance between section 1 and 2	$l_2$	0	m
Width at input height of section 1	$w_{H_1}$	6.2	m
Width at input height of section 3	$w_{H_3}$	5.8	m
<b>Cargo containers (only for visualisation)</b>			
Spanwise spacing between containers	$y_{\text{cargo}}$	0.01	m
Chordwise spacing between containers	$x_{\text{cargo}}$	0.01	m
Type of container(s)		'LD-9'	-
Leading row positioning of containers		[True, True, True]	-
Trailing row positioning of containers		[False, False, False]	-
Number of containers	$n_{\text{containers}}$	None	-
<b>Wing planform</b>			
Wing span	$b$	60.4	m
Planform chord of section 1 fraction	$\bar{c}'_1$	1.16	-
Inboard wing leading edge sweep angle	$\Lambda_{\text{in}}$	64.5	°
Outboard wing leading edge sweep angle	$\Lambda_{\text{out}}$	40.7	°
Dihedral of wing trunk 4	$\Gamma_4$	-0.1785	°
Dihedral of wing trunk 5	$\Gamma_5$	5.825	°
Incidence of aerofoil 4	$i_4$	0.4	°
Incidence of tip aerofoil	$i_5$	-4.37	°
Taper ratio	$\lambda$	0.156	-
Length 4 fraction	$\bar{L}_4$	0.0110	-
Planform chord of section 3 fraction	$\bar{c}'_3$	1.21	-
Angle between aircraft's x axis and aerofoil 4's x axis	$\delta$	52.6	°
<b>Oval</b>			
Cabin height of oval section 1	$H_{2,1}$	2.25	m
Cabin height of oval section 3	$H_{2,3}$	1.75	m
Height of input width of section 1	$H_{w,1}$	0.6	m
Height of input width of section 3	$H_{w,3}$	0.6	m
Crown height of oval section 1	$H_{1,1}$	0.6	m
Crown height of oval section 3	$H_{1,3}$	0.2	m
Keel height of oval section 1	$H_{3,1}$	0.7	m
Keel height of oval section 3	$H_{3,3}$	0.2	m
<b>Rear aerofoil</b>			
Upper rear wing polynomial coefficient of section 1	$c_{\text{up},1}$	1e-5	$\text{m}^{-3}$
Upper rear wing polynomial coefficient of section 3	$c_{\text{up},3}$	1e-5	$\text{m}^{-3}$
Lower rear wing polynomial coefficient of section 1	$c_{\text{low},1}$	0.002	$\text{m}^{-3}$
Lower rear wing polynomial coefficient of section 3	$c_{\text{low},3}$	0.0001	$\text{m}^{-3}$
Vertical position of trailing edge in section 1	$z_{\text{TE},1}$	-0.3	m
Vertical position of trailing edge in section 3	$z_{\text{TE},3}$	-0.04	m
Start position of upper rear wing curve 1	$\tilde{x}_{\text{sup},1}$	0.4	-
Start position of upper rear wing curve 3	$\tilde{x}_{\text{sup},3}$	0.3	-
Start position of lower rear wing curve 1	$\tilde{x}_{\text{low},1}$	0.4	-
Start position of lower rear wing curve 3	$\tilde{x}_{\text{low},3}$	0.3	-
Upper Bernstein coefficients of section 4	$A_{u,4}$	[0.088, 0.066, 0.21, 0.079, 0.24, 0.23]	
Lower Bernstein coefficients of section 4	$A_{l,4}$	[-0.13, -0.084, -0.031, -0.31, 0.069, 0.20]	
Upper Bernstein coefficients of tip section (5)	$A_{u,\text{tip}}$	[0.14, 0.068, 0.20, 0.078, 0.14, 0.29]	
Lower Bernstein coefficients of tip section (5)	$A_{l,\text{tip}}$	[-0.099, -0.084, -0.025, -0.39, 0.061, 0.17]	
<b>Flight mechanics</b>			
Cruise weight	$w_{\text{cruise}}$	2e5	kgf
Cruise Mach number	$Ma_{\text{cruise}}$	0.85	-
<b>Other settings</b>			
Position section by floor		False	-
Number of profiles for torus trunk	$n_{\text{loft}_2}$	10	-
Distance from global origin to wing loft origin	$X_0$	10	m

Table B.4: Input parameters of case 2: a Flying-V-1000

Parameter	Symbol	Value	Unit
Fuselage planform			
Untapered fuselage length (centre line length)	$L_1$	28.75	m
Tapered fuselage length (centre line length)	$L_3$	11.1	m
Leading edge distance between section 1 and 2	$l_2$	0	m
Width at input height of section 1	$w_{H_1}$	6.2	m
Width at input height of section 3	$w_{H_3}$	5.5	m
Cargo containers (only for visualisation)			
Spanwise spacing between containers	$y_{\text{cargo}}$	0.01	m
Chordwise spacing between containers	$x_{\text{cargo}}$	0.01	m
Type of container(s)		'LD-9'	-
Leading row positioning of containers		[True, True, True, True]	-
Trailing row positioning of containers		[False, False, False, False]	-
Number of containers	$n_{\text{containers}}$	None	-
Wing planform			
Wing span	$b$	64.6	m
Planform chord of section 1 fraction	$\bar{c}'_1$	1.17	-
Inboard wing leading edge sweep angle	$\Lambda_{\text{in}}$	64.5	°
Outboard wing leading edge sweep angle	$\Lambda_{\text{out}}$	40.7	°
Dihedral of wing trunk 4	$\Gamma_4$	-0.1785	°
Dihedral of wing trunk 5	$\Gamma_5$	5.825	°
Incidence of aerofoil 4	$i_4$	0.4	°
Incidence of tip aerofoil	$i_5$	-4.37	°
Taper ratio	$\lambda$	0.15	-
Length 4 fraction	$\bar{L}_4$	0.0110	-
Planform chord of section 3 fraction	$\bar{c}'_3$	1.29	-
Angle between aircraft's x axis and aerofoil 4's x axis	$\delta$	59.7	°
Oval			
Cabin height of oval section 1	$H_{2,1}$	2.15	m
Cabin height of oval section 3	$H_{2,3}$	1.27	m
Height of input width of section 1	$H_{w1}$	0.55	m
Height of input width of section 3	$H_{w3}$	0.55	m
Crown height of oval section 1	$H_{1,1}$	0.6	m
Crown height of oval section 3	$H_{1,3}$	0.2	m
Keel height of oval section 1	$H_{3,1}$	0.7	m
Keel height of oval section 3	$H_{3,3}$	0.2	m
Rear aerofoil			
Upper rear wing polynomial coefficient of section 1	$c_{\text{up}1}$	1e-5	$\text{m}^{-3}$
Upper rear wing polynomial coefficient of section 3	$c_{\text{up}3}$	1e-5	$\text{m}^{-3}$
Lower rear wing polynomial coefficient of section 1	$c_{\text{low}1}$	0.002	$\text{m}^{-3}$
Lower rear wing polynomial coefficient of section 3	$c_{\text{low}3}$	0.0001	$\text{m}^{-3}$
Vertical position of trailing edge in section 1	$z_{\text{TE}1}$	-0.3	m
Vertical position of trailing edge in section 3	$z_{\text{TE}3}$	-0.04	m
Start position of upper rear wing curve 1	$\tilde{x}_{\text{sUP}1}$	0.4	-
Start position of upper rear wing curve 3	$\tilde{x}_{\text{sLOW}3}$	0.3	-
Start position of lower rear wing curve 1	$\tilde{x}_{\text{sUP}1}$	0.4	-
Start position of lower rear wing curve 3	$\tilde{x}_{\text{sLOW}3}$	0.3	-
Upper Bernstein coefficients of section 4	$A_{u4}$	[0.088, 0.066, 0.21, 0.079, 0.24, 0.23]	
Lower Bernstein coefficients of section 4	$A_{l4}$	[-0.13, -0.084, -0.031, -0.31, 0.069, 0.20]	
Upper Bernstein coefficients of tip section (5)	$A_{u\text{tip}}$	[0.14, 0.068, 0.20, 0.078, 0.14, 0.29]	
Lower Bernstein coefficients of tip section (5)	$A_{l\text{tip}}$	[-0.099, -0.084, -0.025, -0.39, 0.061, 0.17]	
Flight mechanics			
Cruise weight	$w_{\text{cruise}}$	2e5	kgf
Cruise Mach number	$Ma_{\text{cruise}}$	0.85	-
Other settings			
Position section by floor		False	-
Number of profiles for torus trunk	$n_{\text{loft}2}$	10	-
Distance from global origin to wing loft origin	$X_0$	10	m





## Mesh convergence

Table C.1 contains the values for the mesh control parameters used in the mes convergence study.

Table C.1: Mesh convergence inputs

Parameter						
Nodes per length	7.5	9	10.5	11.25	15	18
Max size wing	0.2	0.17	0.14	0.13	.01	0.08
Outer domain maxim	30	25	21	20	15	13
Triangular element growth rate	0.2	0.17	0.14	0.13	0.10	0.080
Tetrahedral maximum size	30	25	21	20	15	13
Tetrahedral growth rate	0.6	0.5	0.43	0.4	0.3	0.25

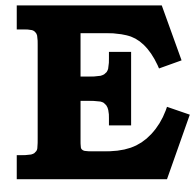


# D

## Design variables and their bounds

Parameter	Symbol	Lower bound	Upper bound	Unit
<b>Wing planform</b>				
Planform chord of section 1 fraction	$\bar{c}'_1$	1	$\frac{L_1 + w_{H_1}}{\tan \Lambda_{in} + 2}$	-
Inboard wing leading edge sweep angle	$\Lambda_{in}$	62	66	°
Outboard wing leading edge sweep angle	$\Lambda_{out}$	18	45	°
Dihedral of wing trunk 4	$\Gamma_4$	-10	+10	°
Dihedral of wing trunk 5	$\Gamma_5$	-10	+10	°
Incidence of aerofoil 4	$i_4$	-10	+10	°
Incidence of tip aerofoil	$i_5$	-10	+10	°
Taper ratio	$\lambda$	0	0.5	
Length 4 fraction	$\bar{L}_4$	0	1	-
Planform chord of section 3 fraction	$\bar{c}_3$	1	$\bar{c}'_1 \frac{w_{H_1} + H_{2_1}}{w_{H_3} + H_{2_3}}$	-
Angle between aircraft's x axis and aerofoil 4's x axis	$\delta$	0	90	°
<b>Oval</b>				
Crown height of oval section 1	$H_{1_1}$	0.1	$\frac{w_{H_1}}{2}$	-
Crown height of oval section 3	$H_{1_3}$	0.1	$\frac{w_{H_3}}{2}$	-
Keel height of oval section 1	$H_{3_1}$	0.1	$\frac{w_{H_1}}{2}$	-
Keel height of oval section 3	$H_{3_3}$	0.1	$\frac{w_{H_3}}{2}$	-
Upper rear wing polynomial coefficient of section 1	$c_{up_4}$	-1e-3	1e-3	$m^{-3}$
Upper rear wing polynomial coefficient of section 3	$c_{up_5}$	-1e-3	1e-3	$m^{-3}$
Lower rear wing polynomial coefficient of section 1	$c_{low_4}$	-1e-3	1e-3	$m^{-3}$
Lower Bernstein coefficients of tip section (5)	$c_{low_5}$	-1e-3	1e-3	$m^{-3}$
Vertical position of trailing edge in section 1	$z_{TE_1}$	-1	1	-
Vertical position of trailing edge in section 3	$z_{TE_3}$	-1	1	-
Start position of upper rear wing curve 1	$x_{sup_1}$	0.1	0.9	-
Start position of upper rear wing curve 3	$x_{slow_3}$	0.1	0.9	-
Start position of lower rear wing curve 1	$x_{sup_1}$	0.1	0.9	-
Start position of lower rear wing curve 3	$x_{slow_3}$	0.1	0.9	-
Upper Bernstein coefficients of section 4	$A_{u_4}$	0	1	
Lower Bernstein coefficients of section 4	$A_{l_4}$	-1	0	
Upper Bernstein coefficients of tip section (5)	$A_{u_{tip}}$	0	1	
Lower Bernstein coefficients of tip section (5)	$A_{l_{tip}}$	-1	0	





## Design space impression

This appendix contains 100 design space samples. The bounds of the design variables are presented in [Appendix D](#).



